Satellite derived leaf area index and roughness length information for surface-atmosphere exchange modelling: a case study for reactive nitrogen deposition in north-western Europe using LOTOS-EUROS v2.0.

Shelley C. van der Graaf[1], Richard Kranenburg[2], Arjo J. Segers[2], Martijn Schaap[2,3], Jan Willem Erisman[1,4]

[1]Cluster Earth and Climate, Department of Earth Sciences, Faculty of Science, Vrije Universiteit Amsterdam, Amsterdam, 1081 HV, The Netherlands

[2]TNO, Climate Air and Sustainability, Utrecht, 3584 CB, The Netherlands

[3]Institute for Meteorology, Free University Berlin, Berlin, 12165, Germany

[4]Louis Bolk Institute, Driebergen, 3972, The Netherlands

Correspondence to: Shelley C. van der Graaf (s.c.vander.graaf@vu.nl)

Abstract. The nitrogen cycle has been continuously disrupted by human activity over the past century, resulting in almost a tripling of the total reactive nitrogen fixation in Europe. Consequently, excessive amounts of reactive nitrogen (N_r) have manifested in the environment, leading to a cascade of adverse effects, such as acidification and eutrophication of terrestrial and aquatic ecosystems, and particulate matter formation. Chemistry transport models (CTM) are frequently used as tools to simulate the complex chain of processes that determine atmospheric N_r flows. In these models, the parameterization of the atmosphere-biosphere exchange of N_r is largely based on few surface exchange measurement and is therefore known to be highly uncertain. In addition to this, the input parameters that are used here are often fixed values, only linked to specific land use classes. In an attempt to improve this, a combination of multiple satellite products is used to derive updated, time-variant leaf area index (LAI) and roughness length (z_0) input maps. As LAI, we use the MODIS MCD15A2H product. The monthly z_0 input maps presented in this paper are a function of satellite-derived NDVI values (MYD13A3 product) for short vegetation types (such as grass and arable land) and a combination of satellite-derived forest canopy height and LAI for forests. The use of these growth-dependent satellite products allows us to represent the growing season more realistically. For urban areas, the z_0 values are updated, too, and linked to a population density map. The approach to derive these dynamic z_0 estimates can be linked to any land use map and is as such transferable to other models. We evaluated the sensitivity of the modelled N_r deposition fields in LOTOS-EUROS v2.0 to the abovementioned changes in LAI and z_0 inputs, focusing on Germany, the Netherlands and Belgium. We computed z_0 values from FLUXNET sites and compared these to the default and updated z_0 values in LOTOS-EUROS. The RMSD for both short vegetation and forest sites improved. Comparing all sites, the RMSD decreased from 0.76 (default z_0) to 0.60 (updated z_0). The implementation of these updated LAI and z_0 input maps led to local changes in the total N_r deposition of up to ~30%

and a general shift from wet to dry deposition. The most distinct changes are observed in land use specific deposition fluxes. These fluxes may show relatively large deviations, locally affecting estimated critical load exceedances for specific natural ecosystems.

1. Introduction

The nitrogen (N) cycle has been continuously disrupted by human activity over the past century (Fowler et al., 2015;Galloway et al., 2004;Galloway et al., 2008), resulting in a doubling of the total reactive nitrogen (N_r) fixation globally and even a tripling in Europe. As a result, excessive amounts of N_r, defined as all N compounds except N_2, have manifested in the environment contributing to acidification and eutrophication of sensitive terrestrial and aquatic ecosystems (Bobbink et al., 2010a;Paerl et al., 2014). NO_x and NH_3 affect air quality through their significant role in the formation of particulate matter, impacting human health and life expectancy (Lelieveld et al., 2015;Bauer et al., 2016;Erisman and Schaap, 2004). N_r also influences climate change through its impact on greenhouse gas emissions and radiative forcing (Erisman et al., 2011;Butterbach-Bahl et al., 2011). As N_r forms are linked through chemical and biological conversion in one another within the environmental compartments, one atom of N may even take part in a cascade of N_r forms and effects (Galloway et al., 2003). To minimize these adverse effects, effective nitrogen management and policy development, therefore, require consideration of all N_r forms simultaneously.

With the scarceness and inadequate distribution of available ground measurements, especially for reduced N_r, the most important method to assess and quantify total N_r budgets on a larger spatial scale to date remains the use of models. Models, chemistry transport models, in particular, are used for understanding the atmospheric transport and the atmosphere-biosphere exchange of nitrogen compounds. Most chemistry transport models compare reasonably with observations for oxidized forms of N_r, but need improvement when it comes to the reduced forms of N_r (Colette et al., 2017). Modelled NH_3 fields are in general uncertain due to the highly reactive nature and the uncertain lifetime of NH_3 in the atmosphere. More importantly, NH_3 emissions that are used as model input are very complex to estimate and remain highly uncertain (Reis et al., 2009;Behera et al., 2013), for example, due to the diversity in NH_3 volatilization rates originating from different agricultural practices. Recently, a lot of effort has been made to improve the spatiotemporal distributions of bottom-up NH_3 emissions (e.g. (Hendriks et al., 2016;Skjøth et al., 2011)). Emissions can also be estimated top-down through the usage of data assimilation and inversion techniques. Optimally combining observations and chemistry transport models have already enabled us to create large-scale emission estimates for various pollutants (e.g. (Curier et al., 2014;Abida et al., 2017)), for instance for NO_2, and will likely also be used for large-scale NH_3 emission estimates in the future.

Most data assimilation and inversion methods rely on the assumption that sink terms in the model hold a negligible uncertainty. To obtain reasonable top-down emission estimates, we must thus also aim to reduce the uncertainty involved on this side of models. The sink strengths of trace gases and particles in chemistry transport models are often pragmatic and computed with relatively simple empirical functions (e.g. following (Wesely, 1989;Emberson et al., 2000;Erisman et al., 1994)), mostly linked to land use classification maps. The parameterization of the

atmosphere-biosphere exchange of N_r components that is used in models is largely based on surface exchange measurements and is therefore very uncertain, especially for NH_3 (Schrader et al., 2016). The deposition strengths in models may vary tremendously depending on the used deposition parameterisation and velocities (Wu et al., 2018;Schrader and Brummer, 2014;Flechard et al., 2014). Moreover, inter-model discrepancies in deposition fluxes may also arise from differences in the used input variables. Here, we focus on the leaf area index (LAI) and the roughness length (z_0) input values. The deposition velocity is often parameterized using both the LAI and the z_0. Currently, most models use fixed, land use specific values for both parameters. In practice, however, spatial as well as seasonal variation is observed. In this paper, we aim to improve the deposition flux modelling by using more realistic, spatial- and time-variant LAI and z_0 values that are derived from optical remote sensors.

The LAI is defined as the one-sided green leaf area per unit surface area (Watson, 1947). The LAI serves as a measure for the amount of plant canopy, and herewith directly related to energy and mass exchange processes. As a result, the LAI is nowadays used as one of the main parameters in many ecological models. In deposition modelling, stomatal uptake is often parameterised using the LAI. The LAI can be determined in the field using either direct methods, such as leaf traps, or indirect methods, such as hemispherical photography (Jonckheere et al., 2004). For larger areas, the LAI can be simulated using land surface or biosphere models. Another group of indirect methods to estimate the LAI for large regions is the use of optical remote sensing. The LAI can, for instance, be estimated using empirical relationships between LAI and vegetation indices (e.g. (Soudani et al., 2006;Davi et al., 2006;Turner et al., 1999)) or by inversion of canopy reflectance models (e.g. (Houborg and Boegh, 2008;Myneni et al., 2015)). A well-known example of the latter is the LAI product from the MODIS instrument, which we will use in this study.

The z_0 is used to describe the surface roughness. The surface roughness serves as a momentum sink for atmospheric flow and is, therefore, an important term in atmospheric modelling. The interaction between the boundary layer and the roughness of the Earth's surface results in shear stress that affects the wind speed profile. Under neutral conditions the resulting wind profile can be approximated using a logarithmic profile:

$$U(z) = \frac{u_*}{k} ln\left(\frac{z}{z_0}\right) \quad \text{(eq. 1)}$$

$U(z)$ represents the mean wind speed, u_* the friction velocity and k the Von Kármán constant. Here, z_0 is a constant that represents the height at which the wind speed theoretically becomes zero. The z_0 can be estimated from in-situ wind speed measurements using bulk transfer equations. More recently, several studies have shown that z_0 for specific, uniform land cover types can also be estimated from optical remote sensing measurements, for instance using vegetation indices (e.g. (Xing et al., 2017;Yu et al., 2016;Bolle and Streckenbach, 1993;Hatfield, 1988;Moran, 1990)). The z_0 can also be estimated using (satellite-derived) vegetation height (e.g. (Raupach, 1994;Plate, 1971;Brutsaert, 2013;Schaudt and Dickinson, 2000)).

The use of optical remote sensing data holds promising potential for improvements of the representativeness of the surface characterization in chemistry transport models. Here, we present an approach to derive monthly z_0 input maps using satellite-derived NDVI values (MYD13A3 product) for short vegetation types and a combination of

satellite-derived forest canopy height and LAI for forests. We validate these z_0 values by comparing them to z_0 values computed from FLUXNET observations. We also update the z_0 values for urban areas, using a population density map. We use the updated z_0 values, as well as the MODIS-LAI, as input in LOTOS-EUROS to illustrate the effect on transport and deposition modelling of N_r components. We evaluate the sensitivity of the N_r deposition fields to these input parameters, focusing on Germany, the Netherlands and Belgium. Moreover, we quantify and present the implications for land use specific fluxes on a model subpixel level. Also, we compare our model outputs with wet deposition measurements of NH_4^+ and NO_3^- and surface concentration measurements of NH_3 and NO_2.

2. Model and datasets

2.1. LOTOS-EUROS

2.1.1. Model description

The LOTOS-EUROS model is a Eulerian chemistry transport model that simulates air pollution in the lower troposphere (Manders et al., 2017). In this study the horizontal resolution is set to 0.125º by 0.0625º, corresponding to pixels of approximately 7 by 7 kilometres in size. The model uses a five-layer vertical grid that extends up 5 km above sea level, starting with a surface layer with a fixed height of 25 meters. The next layer is a mixing layer, followed by two time-varying dynamic reservoir layers of equal thickness, and a top layer up to 5 km. LOTOS-EUROS follows the mixed layer approach and performs hourly results using ECMWF meteorology (European Centre for Medium-Range Weather Forecasts, 2016). The gas-phase chemistry uses the TNO CBM-IV scheme (Schaap et al., 2009) and the anthropogenic emissions from the TNO-MACC-III emission database (Kuenen et al., 2014). The wet deposition parameterisation is based on the CAMx approach, and includes both in-cloud and below-cloud scavenging (Banzhaf et al., 2012). LOTOS-EUROS makes use of the CORINE/Smiatek land use map to determine input values for surface variables.

2.1.2. Dry deposition

The dry deposition flux of gases is computed following the resistance approach, in which the exchange velocity V_d is equal to the reciprocal sum of the aerodynamic resistance R_a, the quasi-laminar boundary layer resistance R_b and the canopy resistance R_c:

$$V_d = \frac{1}{R_a + R_b + R_c} \quad \text{(eq. 2)}$$

R_a and R_b are both influenced by the wind profile, which is computed with (eq. 1). The wind profile, in turn, depends on roughness length z_0 associated with different land use classes. The aerodynamic resistance R_a is computed as follows:

$$R_a = \int_{z_0}^{h} \frac{\Phi\left(\frac{z}{L}\right)}{\kappa u_* z} dz \quad \text{(eq. 3)}$$

Here, h is the canopy height, which is pre-defined per land use class. The empirical function $\Phi\left(\frac{z}{L}\right)$ is taken from Businger et al. (1971) and depends on the state of the atmosphere. Depending on the value of Monin-Obukhov length L, the following equations are used:

For a stable atmosphere ($L > 0$): $\Phi_s\left(\frac{z}{L}\right) = 1 + 4.7\left(\frac{z}{L}\right)$ (eq. 4)

For an unstable atmosphere ($L < 0$): $\Phi_u\left(\frac{z}{L}\right) = \left(1 - 15\left(\frac{z}{L}\right)\right)^{-0.25}$ (eq. 5)

For a neutral atmosphere is it equal to unity. The Monin-Obukhov length L is dependent on z_0, and is determined as follows:

$$\frac{1}{L} = S\left(a_1 + a_2 S^2\right) z_0^{\left(b_1 + b_2|S| + b_3 S^2\right)} \quad \text{(eq. 6)}$$

Here, a_1, a_2, b_1, b_2 and b_3 are constants (0.004349, 0.003724, -0.5034, 0.2310 and -0.0325 respectively) and $S = -0.5\left(3.0 - 0.5\, u_s|CE|\right)$ with near-surface wind speed u_s and exposure factor CE, depending on cloud cover and solar zenith angle. The wind speed at a reference height (10 meters) is used to obtain the friction velocity u_*:

$$u_* = \kappa u_{10m} / \ln\left(\frac{z_{10m}}{z_0}\right) \quad \text{(eq. 7)}$$

The quasi-laminar boundary layer resistance R_b is a function of the cross-wind leaf dimension L_d and the wind speed at canopy top, $u(h)$, following the parameterisation presented in McNaughton and Van Den Hurk, 1995:

$$R_b = 1.3 * 150 * \sqrt{\frac{L_d}{u(h)}} \quad \text{(eq. 8)}$$

L_d is set to 0.02 m for arable land and permanent crops, and to 0.04 m for deciduous and coniferous forests. For other land use classes L_d, and subsequently, the R_b, is equal to zero. The canopy resistance R_c is computed using the DEPAC3.11 (Deposition of Acidifying Compounds) module (van Zanten et al., 2010). R_c is a parallel system of the resistances of three different pathways, the external leaf surface or cuticular resistance R_w, the effective soil resistance $R_{soil,eff}$ and the stomatal resistance R_s, and is defined as:

$$R_c = \left(\frac{1}{R_w} + \frac{1}{R_{soil,eff}} + \frac{1}{R_s}\right)^{-1} \quad \text{(eq. 9)}$$

The external leaf surface resistance R_w is a function of the surface area index (SAI) and the relative humidity. The SAI is a function of the LAI. The effective soil resistance $R_{soil,eff}$ is the sum of the in-canopy resistance R_{inc} and the soil resistance R_{soil}. Soil resistance R_{soil} has a fixed value, depending on the land use class and conditions (frozen, wet or dry). In case of $u_* > 0$ the in-canopy resistance for arable land, permanent crops and forest is computed as follows:

$$R_{inc} = \frac{14\ h\ SAI}{u_*} \quad \text{(eq. 10)}$$

For $u_* < 0$ and other land use classes a fixed value is used. The stomatal conductance for optimal conditions is the product of the LAI and the maximum leaf resistance from (Emberson et al., 2000). This maximum value is reduced by correction factors for photoactive radiation, temperature and vapor pressure deficit to obtain the stomatal conductance G_s. The R_s is then equal to $1/G_s$. The resistance parameterizations differ with land us type. A total of nine different land use classes are used in DEPAC. LOTOS-EUROS uses a fixed z_0 value for each of these land use classes. The default LAI values are also linked to the DEPAC classes, and follow a fixed temporal behaviour that describes the growing season of each land use class (Emberson et al., 2000). The bi-directional exchange of NH_3 is included in the implementation of the DEPAC3.11 module (Wichink Kruit et al., 2012), allowing emissions of NH_3 under certain atmospheric conditions. More information about the most recent version of the model can be found in Manders et al. (2017).

2.2. Datasets

The following section gives a short description of all the datasets that are used in this study. Firstly, a description of the LAI dataset is given. Subsequently, the datasets that are used to derive the updated z_0 maps are described. Finally, the in-situ observations used for validation are discussed in the last paragraphs.

2.2.1. MCD15A2H Leaf Area Index

The satellite-derived Leaf Area Index (LAI) is a combined product of the MODIS instruments on board the Terra and Aqua satellites (Myneni et al., 2015). The LAI algorithm compares bidirectional spectral reflectances observed by MODIS to values evaluated with a vegetation canopy radiative transfer model that are stored in a look-up table. The algorithm then archives the mean and the standard deviation of the derived LAI distribution functions. We used the 6th version of the product, MCD15A2H, which has a temporal resolution of 8 days and a spatial resolution of 500 meters.

2.2.2. MYD13A3 NDVI

The Normalized Difference Vegetation Index (NDVI) is a vegetation index computed with reflectances observed by the MODIS instrument on board of the Aqua satellite (Didan, 2015). The NDVI is the normalized transform of the near infrared to the red reflectance and is expressed by:

$$\mathrm{NDVI} = \frac{\rho_{\mathrm{NIR}} - \rho_{\mathrm{red}}}{\rho_{\mathrm{NIR}} + \rho_{\mathrm{red}}} \quad \text{(eq. 3)}$$

We used the MYD13A3 product, which is the monthly NDVI product with a spatial resolution of 1 km.

2.2.3. Forest canopy height

The forest canopy height is derived from LIDAR (Light Detection And Ranging) data acquired by the GLAS (Geoscience Laser Altimeter System) instrument aboard the ICESat (Ice, Cloud, and land Elevation Satellite) satellite (Zwally et al., 2002). This instrument was an altimeter that transmitted a light pulse of 1024 nm and recorded the reflected waveform. We used the global forest canopy height product developed by Simard et al. (2011), which has a spatial resolution of 1 km.

2.2.4. Population density map

The population density grid used in this study available for all European countries and provided by the European Environmental Agency (Gallego, 2010). The population density is disaggregated with the CORINE Land Cover inventory of 2000, using data on population per commune. The resulting population density grid is downscaled to a spatial resolution of 100 meters.

2.2.5. CORINE Land Cover

The CORINE Land Cover (CLC) is a land use inventory that consists of 44 classes (European Environmental Agency, 2014). The CLC is produced by computer-assisted visual interpretation of a collection of high resolution satellite images. The CLC has a minimum mapping unit of 25 ha and a thematic accuracy of >85%. We used the latest version of the product, CLC 2012, in this study.

2.2.6. In-situ reactive nitrogen observations

The modelled NH_4^+ and NO_3^- wet deposition fluxes are compared to observations of wet-only samplers. We used observation from the Dutch LMRe network (Van Zanten et al., 2017) and the German Lander network (Schaap et al., 2017).The location of the stations can be found in Figure 16. The modelled NH_3 surface concentrations are compared to observation from the Dutch MAN network (Lolkema et al., 2015) and the European EMEP network (EMEP, 2016). The modelled NO_2 surface concentrations are compared to observation from AirBase (EEA, 2019). We only used background stations. The location of these stations can be found in Figure 14.

2.2.7. Eddy covariance data

FLUXNET is a global network of micrometeorological towers that measure biosphere-atmosphere exchange fluxes using the eddy covariance (EC) method. We used half-hourly observations from the FLUXNET2015 dataset (Pastorello et al., 2017) to validate the z_0 values. We use observations of the mean wind speed, the friction velocity, the sensible heat flux, precipitation and air temperature T_a to determine z_0 values . The sites used in this study are shown in Table 1.

3. Methodology

3.1. Updated z_0 maps

The updated z_0 maps are a composition of z_0 values derived using different methods. We distinguish three different main approaches: 1) z_0 values that depend on forest canopy height, 2) z_0 values that depend on the NDVI and 3) new

z_0 values for urban areas that depend on the population density map. In addition to these three approaches, the z_0 values of some urban classes were set to new default values. An overview of the datasets that are used for each DEPAC land use class is given in Table 2.

The MODIS NDVI, the MODIS LAI and the GLAS forest canopy height had to be pre-processed and homogenized in order to obtain consistent input maps that can be read into the LOTOS-EUROS model. To achieve this, we created input maps for each DEPAC class on the coordinate grid of the CORINE/Smiatek land use map in LOTOS-EUROS.

First of all, the original datasets were re-projected to geographic coordinates. The following approach is used to deal with the different horizontal resolutions of the datasets: We used the CLC2012 map, having the highest horizontal resolution, as a basis for the computation of the updated z_0 values. For each of the other datasets, we first computed the percentages of each CORINE land cover class within every pixel. We define homogeneous pixels, consisting of nearly one CORINE land cover class, for which we will use a threshold value of 85% of the pixels area. Then we isolate and use only these (nearly) homogeneous pixels to compute z_0 values for each CORINE land cover class. The methods that were applied are described in the subsequent section.

3.1.1. Forest canopy height derived z_0 values

The forest canopy height dataset derived from GLAS LiDAR observations is used to compute the z_0 values for each CLC2012 forest land cover class (broad-leaved forest, coniferous forest and mixed forest) that corresponds to one of the DEPAC forest land use classes (4: coniferous forest and 5: deciduous forest). Several publications relate vegetation height to z_0 (e.g. (Raupach, 1994;Plate, 1971;Brutsaert, 2013)). Here we used the often used equation from (Brutsaert, 2013):

$$z_0 = 0.136 * h \qquad \text{(eq. 4)}$$

The vegetation height is the most important parameter influencing turbulence near the surface, and for this reason, the used parameterisation gives a reasonable estimate of z_0, even though it ignores many other aspects that influence z_0 (e.g. density, vertical distribution of foliage). Multiple studies have illustrated that there is a seasonal variation in z_0/h for different types of forests (e.g. (Yang and Friedl, 2003;Nakai, 2008)). The z_0 of deciduous trees is therefore additionally linked to the leaf area index to account for changes in tree foliage. The following formula is used to compute the monthly z_0 value for each deciduous forest pixel:

$$z_0(LAI) = z_{0,min} + \frac{LAI - LAI,min}{LAI,max - LAI,min} (z_{0,max} - z_{0,min}) \qquad \text{(eq. 5)}$$

Here the maximum roughness length $z_{0,max}$ is set to the LiDAR-derived z_0 from (eq. 4). The minimum roughness length $z_{0,min}$ represents the z_0 of leafless deciduous trees. Following the dependence of z_0/h on LAI presented in Nakai (2008) and Yang and Friedl (2003), we set the $z_{0,min}$ to 80% of $z_{0,max}$.

3.1.2. NDVI derived z_0 values

Table 3 gives an overview of several studies that relate the z_0 value to the NDVI. The functions are derived for different vegetation types under specific conditions. Equations 6 to 12 are derived for different types of agricultural land. These equations are all within a reasonable range from one another for NDVI values below ~0.8. Therefore, we chose to use the average function of eq. 6 to eq. 11 to compute z_0 values for all CLC subcategories of the following DEPAC classes: "arable", "other" and "permanent crops". Figure 1 is a visualization of eq. 6 to 11 and the used mean function. Figure S1 shows histogram of all NDVI values in our study area in 2014. We computed that 7.4% of all NDVI values have a NDVI > 0.8, 1.3% have a NDVI > 0.85 and only 0.04% have a NDVI > 0.9. Virtually all NDVI values thus fall within the range where the average function does not differ much from the individual functions. The z_0 value of grasslands is in general lower than other vegetation types. The last equation, eq. 12, is specifically derived for grassland and is therefore used for all CLC subcategories that fall under the DEPAC class "grass".

3.1.3. z_0 values for urban areas

The default z_0 of urban areas in LOTOS-EUROS was set to 2 meters. We have updated the z_0 values for urban areas to avoid possible overestimation of z_0 in sparsely populated urban areas. The updated z_0 values for CLC2012 class 1 and 2, '1: continuous urban fabric' and '2: discontinuous urban fabric' are time-invariant and coupled to the EEA population density map. The z_0 values are set to 2 metres in areas with a population density higher than 5000 inhabitants/km^2 and to 1 metre in areas with a population density lower than 5000 inhabitants/km^2. The z_0 values of the other urban subcategories, CLC2012 class 3 to 9, are updated to the proposed values for CLC classes in (Silva et al., 2007). Figure S2 shows the resulting updated z_0 values for urban areas.

3.2. LAI and z_0 in LOTOS-EUROS

After the computation of the z_0 values, the maps for each CORINE land cover class were merged and converted into DEPAC classes using a pre-defined conversion table. As multiple CORINE land cover may translate to one single DEPAC class, the weighted average based on the respective percentage of each CORINE land cover class was computed for each pixel. We then used linear interpolation to obtain continuous z_0 maps for each DEPAC class. Finally, the maps were re-gridded unto the CORINE/Smiatek grid and saved into one file per month.

The default parameterization of the LAI in LOTOS-EUROS is replaced by the MCD15A2H LAI product from MODIS. First, we applied a coordinate transformation to obtain the data in geographical coordinates. The data was then re-gridded unto the grid of the CORINE/Smiatek land use map using linear interpolation. The quality tags were evaluated to identify pixels with default fill values from the MCD15A2H product. These fill-values were replaced by the default LAI values in LOTOS-EUROS, to avoid modelling discrepancies resulting from sudden jumps in LAI values. Finally, the values were sorted per DEPAC land use class and individual fields were created for each class as new input for LOTOS-EUROS.

3.3. z_0 values from EC measurements

We used the regression method (e.g. Graf et al., 2014. Chen et al., 2015) to compute z_0 from several eddy covariance sites. A description of the methodology and the data processing is given in this section. The wind profile in the surface layer can be approximated by:

$$\ln\left(\frac{z-d}{z_0}\right) = \frac{k\,u(z)}{u^*} + \Psi_m\left(\frac{z-d}{L}\right) \quad \text{(eq. A)}$$

here, z is the measurement height, d is the displacement height, z_0 is the aerodynamic roughness length, k is the Von-Karman constant (=0.4), $u(z)$ is the average wind speed, u^* is the friction velocity and Ψ_m is the integrated universal momentum function, also known as the stability correction term. Ψ_m is a function of L, the Monin-Obukhov length, which is defined as (e.g. Erisman and Duyzer, 1991):

$$L = -\frac{u_*^3\,T_a\rho c_p}{kgH} \quad \text{(eq. A)}$$

where T_a is the air temperature, ρ the air density (= 1.2 kg m^{-3}), c_p the heat capacity at constant pressure (=1005 J kg^{-1} K^{-1}), g the acceleration due to gravity, and H the sensible heat flux. Stability correction term Ψ_m is in principle a non-linear function, however, for a certain stability range it can be approximated by a linear function. It is shown that for moderately stable conditions ($0 < \frac{z-d}{L} < 1$) stability correction term Ψ_m holds the following form:

$$\Psi_m\left(\frac{z-d}{L}\right) = -\beta * \left(\frac{z-d}{L}\right) \quad \text{(eq. A)}$$

where β is a constant. We consider a simple linear regression with offset parameter a and slope parameter b. If we assume that Ψ_m is linear, we can rewrite Eq. 1 in the following form:

$$\frac{k\,u(z)}{u^*} = a + b\left(\frac{z-d}{L}\right) \quad \text{(eq. A)}$$

Now a provides an estimate of $\ln(z-d)/z_0$, and we can directly compute z_0 from $(z-d)/\exp(a)$. We use observations from 2014 only, unless stated otherwise in Table 1. For forest we assume that $d = (2/3) * h$ (Maurer et al., 2013), and we use the forest canopy height derived from GLAS. For short vegetation we assume that displacement height d is negligible, that is, $d = 0$. Graf et al., 2014 illustrated that the linearity approximation of Ψ_m is valid for small negative values of $(z-d)/L$, so we first select all points where -0.1 < $(z-d)/L$ < 1. We filter out observation during rainfall and where $u^* < 0.15$, as presented in Chen et al., 2015. We split our data into a group with stable conditions ($L > 0$) and with unstable conditions ($L < 0$). We assume that the z_0 is more or less constant over a period of 5 days. For each 5-day period we plot $ku(z)/u^*$ against $(z-d)/L$ and fit a simple line function using linear least-squares. The z_0 values are then computed from offset parameter a. We compute the mean, median, standard deviation and the range of the all computed z_0 values in one year. If the computed z_0 values for

stable and unstable conditions in one 5-day period differ more than 50% from their arithmetic mean they are filtered out.

4. Results

4.1. Comparison of the default and updated z_0 values

We used the CORINE/Smiatek land use map to combine all the updated z_0 values into one single map. The resulting composite map has a horizontal resolution of 500 by 500 metres and is shown in Figure 2.

The mean relative difference (MRD) between the default and updated z_0 values is presented in Figure 3. The largest positive differences occur in forested areas, meaning that the default z_0 values are lower than the updated z_0 values. The largest negative deviations occur in urban areas and areas with "grass". The updated z_0 values are generally lower in the Netherlands and Belgium, and mostly higher in Germany. Table 4 gives an overview of the default z_0 values in LOTOS-EUROS and the mean and standard deviation of the new z_0 values for each of the DEPAC land use classes. The updated z_0 values for "arable land", "coniferous forest", "deciduous forest" and "other" are on average higher than the default z_0 values in LOTOS-EUROS. The updated z_0 values for "grass", "permanent crops" and "urban" are on average lower than the default z_0 values in LOTOS-EUROS.

4.2. Comparison to z_0 values from other studies

We compared the updated z_0 values to z_0 values from several studies (Wieringa, 1993;Silva et al., 2007;Troen and Petersen, 1989;Lankreijer et al., 1993;Yang and Friedl, 2003), and z_0 values used in other CTMs (Simpson et al., 2012;Mailler et al., 2017). Table 5 gives an overview of these z_0 values. There is in general good agreement with these z_0 values, and the updated z_0 values mostly fall within the stated ranges. The updated z_0 values for coniferous and deciduous forest are on the high side compared to these studies. A histogram of the forest canopy heights derived from GLAS within our study area is given in Figure S1. These differences can in part be explained by the occurrence of relatively tall forest canopy (~30 meters) in the dataset, especially in forest in southern Germany, whereas most of these studies either assumed or studied shorter trees. Another possible explanation lies in the fact that we used a relatively large conversion factor of 0.136 (eq. 4), whereas a factor of 0.10 is also used quite often.

4.3. Comparison to z_0 values derived from EC measurement sites

We computed the z_0 values of the EC sites. We compared the z_0 values based on their land use stated by FLUXNET, to avoid issues arising from discrepancies in land use classifications. The forest sites (DBF, ENF and MF) are compared to z_0 values derived from GLAS. The cropland and wetland sites (CRO and WET) are compared to the NDVI-dependent z_0 values derived using the mean function shown in Figure 1. The grassland sites (GRA) are compared to the NDVI-dependent z_0 values for grassland specifically. The results per site are given in Table 6. Figure 4 shows the comparison of the z_0 values from EC measurements and the updated z_0 values for different land use classes. The z_0 values for forest match quite well. The z_0 values for short vegetation seem to be overestimated for crops and underestimated for grassland and wetland sites. The underestimation of some grassland and wetland

sites can be explained by the large inter-site differences in vegetation cover. Some of the FLUXNET sites classified as grasslands are for instance mostly covered with short grass only (for instance Oensingen), whereas there are also sites with relatively tall herbaceous vegetation, such as reeds (for instance Horstermeer). Compared to the default z_0 values in LOTOS-EUROS, the root-mean-square difference (RMSD) improved from 0.76 (default z_0) to 0.60 (updated z_0). For forest, the RMSD decreased from 1.23 (default z_0) to 0.96 (updated z_0). For short vegetation, the RMSD also decreased, from 0.22 (default z_0) to 0.19 (updated z_0). Figure 5 shows the comparison of the seasonal variation in computed and satellite-derived z_0 values for the FLUXNET sites classified as crops in 2014. We can once more observe a clear offset between the two. The FLUXNET z_0 values go to near-zero values in wintertime, whereas the satellite-derived z_0 values never drop below 0.12 meters. This seems to be due to the distribution of the NDVI values (Figure S1), which shows that the NDVI > 0.4 most of the time. The seasonal patterns, on the other hand, seem to match well in general, even though the satellite-derived z_0 values rise somewhat earlier in the year.

4.4. Comparison of the default and MODIS LAI

The yearly mean MODIS LAI values are shown in Figure 6. The mean differences between the MODIS and the default LAI values are presented in Figure 7. The largest positive differences occur in areas with “arable land”, where the mean default LAI values are lower than the MODIS LAI values. The largest negative deviations occur in areas with forest, especially for “coniferous forest”. The seasonal variation of the MODIS and the default LAI values are shown in Figure 8. The default LAI of “grass” and “deciduous forest” seems to fit the yearly variation of the MODIS LAI quite well. We matched the MODIS-LAI with the locations of the FLUXNET sites to take a closer look at the pattern for different land use classes. Figure 9 shows the seasonal variation of the MODIS-LAI at FLUXNET sites with different land use classifications. The LAI of the grassland sites seems to vary the most, which corresponds to the large inter-site differences in vegetation cover. For the cropland sites, we can recognize the growing season and the apparent harvest, where the LAI values drop again. Of all the different land use classes, deciduous broadleaf forest sites reach the highest LAI values in the growing season. There is less variation in the LAI for evergreen needle leaf forest sites. However, the wintertime LAI values seem to be unrealistically low.

4.5. Implications for modelled N_r deposition fields

In the following section, the impact of the updated LAI and z_0 values on modelled N_r deposition fields in LOTOS-EUROS is discussed. A total of four different LOTOS-EUROS runs are compared to examine the individual effect of the updated LAI and z_0 values on the modelled N_r distributions and deposition fields. The first run, named “$LE_{default}$”, is the standard run using default LAI and z_0 values. The second run, named “LE_{LAI}”, uses updated LAI values and the default z_0 values. The third run, named “LE_{z0}”, uses updated z_0 values and the default LAI values. The fourth run, named “LE_{z0+LAI}”, uses both updated LAI and z_0 values. From now on, we will refer to the outputs of these different runs using the abovementioned abbreviations.

4.5.1. Effect on total N_r deposition

Figure S3 shows the division of the total terrestrial N_r deposition over Germany, the Netherlands and Belgium into different N_r compounds for each of the model runs. A relatively larger portion of the total N_r deposition is attributed to oxidized forms of N_r in Germany. The reduced forms of N_r predominate in the Netherlands and Belgium. The largest change in total N_r deposition occurs in Belgium (+6.19%) due to the inclusion of the MODIS LAI. This corresponds to the relative increase in LAI values here. The inclusion of the updated z_0 values lead to a minor decrease in total N_r deposition in the Netherlands (-1.45%) and Belgium (-1.13%), and a minor increase in Germany (+0.44%).

4.5.2. Effect on wet and dry N_r deposition

We examined the direct effect of the updated LAI and z_0 values on the modelled dry N_r deposition, as well as the related indirect effect in modelled wet N_r deposition. Figure 10 shows the dry and wet N_r deposition in kg N ha^{-1} in 2014, modelled with the updated LAI and z_0 values as input in LOTOS-EUROS. Figure 11 shows the relative changes in the total amount of dry and wet N_r deposition of the different runs with respect to the default run. The combined effect shows an increase of the amount of dry N_r deposition over most parts of Belgium and Germany. The amount of wet N_r deposition decreases over most parts of Germany and eastern Belgium, but remains unchanged in north-western parts of Germany. We observe a decrease in total N_r deposition in the Netherlands. In general, we observe changes ranging from approximately -20% to +30% in the total amount of dry N_r deposition. The changes in wet N_r deposition are smaller in magnitude and range from approximately -3% to +3%.

4.5.3. Effect on reduced and oxidized N_r deposition

We split up the total Nr deposition into NH_x (NH_3 and NH_4^+) and NO_y (NO and NO_2 and NO_3^- and HNO_3) deposition, to look at the effect of the updated LAI and z_0 input maps on the deposition of reduced and oxidised forms of N_r, respectively. Figure 12 shows the modelled NH_x and NO_y deposition in kg N ha^{-1} in 2014, including the updated LAI and z_0 input values. Figure 13 shows the relative changes (%) in the total NH_x and NO_y of the different runs with respect to the default run of LOTOS-EUROS. The updated z_0 values have a larger impact on the NH_x deposition than on the NO_y deposition. The implementation of the updated z_0 values has led to a decrease in NH_x deposition over most of the Netherlands, and western Belgium, driven by the large fraction of grassland here. The updated LAI values led to relatively more NH_x deposition in Belgium. The updated LAI values led to an increase of NO_y deposition in almost all areas within the modelled region, except for some urban areas. Moreover, the impact seems to be limited in large forests located in background areas.

4.5.4. Effect on land use specific fluxes

Table 7 gives an overview of changes in the distribution of the land use specific fluxes in the whole study area (Germany, the Netherlands and Belgium combined) for the different runs. The most distinct changes in N_r deposition are due to the updated LAI values ("LE_{LAI}"), where we observe an increase in total N_r deposition on urban areas (+ 16.62%) and arable land (+ 9.53%), and a decrease on coniferous forests (- 9.36%). This coincides with the categories where we observe the largest changes in LAI values. The default LAI values in urban areas were

first set to zero for all urban DEPAC categories. The MODIS LAI values, however, are only zero in densely populated areas and areas with industry. The main effects of the updated z_0 values ("LE_{z0}") can be observed for grass (-3.95 %), permanent crops (+ 3.27) and arable land (-3.17 %). In the combined run, "LE_{z0+LAI}", we observe an amplified effect in total N_r deposition over grass (- 8.05%) and arable land (+ 12.88%). The impact of the individual parameters on the remaining land use categories is attenuated in this run.

4.6. Implications for N_r distributions

The changes in N_r deposition amounts induce an effect in the modelled distribution of nitrogen components. Here, we look at the effect of the updated LAI and z_0 values on NH_3 and NO_2 surface concentrations. Figure 14 shows the updated modelled NH_3 and NO_2 surface concentrations in 2014. The dots on top of the figures represent the stations that are used for validation, and their observed mean NH_3 and NO_2 surface concentrations. Figure 15 shows the relative change in yearly mean NH_3 and NO_2 surface concentrations in 2014 of the different runs with respect to the default run of LOTOS-EUROS.

The first column represents the changes in NH_3 and NO_2 surface concentrations due to the updated z_0 values. The NH_3 surface concentration in the Netherlands has increased by up to ~8%. The NH_3 surface concentration in almost all of Germany has decreased by up to ~10%. The changes in the NO_2 surface concentration are less distinct and changed approximately minus to plus 4% in most areas. The middle column represents the changes in NH_3 and NO_2 surface concentrations due to the inclusion of the MODIS LAI only. The NH_3 surface concentration has increased with up to ~10% in the Netherlands, western Belgium and north-western and southern Germany. The NH_3 surface concentration has decreased in eastern Belgium and central Germany. The NO_2 surface concentrations have decreased with up to ~6% in almost all of the modelled area.

4.7. Comparison to in-situ measurements

To analyse the effect of the updated LAI and z_0 values, we compared our model output to the available in-situ observations. Due to the lack of available dry deposition measurements, we decided to use NH_4^+ and NO_3^- wet deposition and NH_3 and NO_2 surface concentrations measurements instead. The distribution of the wet deposition stations is shown in Figure 16, as well as the modelled mean NH_4^+ (left) and NO_3^- (right) wet deposition in 2014. The locations of the stations that measure the NH_3 and NO_2 surface concentrations are shown in Figure 14.

The relationships between the modelled and observed fields are evaluated using the Pearson's correlation coefficient (r), the RMSD and the coefficients (slope, intercept) of simple linear regression. Table S1 shows these measures for the comparison with monthly mean NO_3^- wet deposition, NH_4^+ wet deposition, and the monthly mean NH_3 and NO_2 surface concentrations in 2014. Table S1 shows the same statistics but computed per DEPAC land use class. Overall, we do not observe large changes in the shown measures due to the inclusion of the updated LAI and z_0 values on a yearly basis. The model underestimates NO_3^- wet deposition, and NH_4^+ to a lesser extent, too. The modelled NH_3 surface concentrations are in general higher than observed concentrations. The opposite is true for

NO_2, here, the modelled surface concentrations are lower than the observed concentrations. The computed measures did not change drastically due to the inclusion of the updated z_0 and LAI values.

Figure S4 shows the monthly mean NO_3^- wet deposition, NH_4^+ wet deposition, NH_3 surface concentration and NO_2 surface concentrations for the different model runs and the mean of the corresponding in situ observations. The relative changes with respect to the default model run are shown in the bottom figures. For NH_4^+, the model captures the observed pattern quite well, although the mean spring peak has slightly shifted. The model captures the monthly variation of NO_3^- well in general, too. There appears to be an underestimation during the winter, especially in December. The observed NH_3 surface concentrations are lower than the modelled concentrations at the beginning of spring and higher during summer. The measured NO_2 surface concentrations are continuously higher than the modelled values. A potential reason for this might be the spread of the NO_2 stations. Unlike NH_3, NO_2 is not only measured in nature areas but all types of locations. Even the selected background stations may, therefore, be located relatively closer to emission sources, leading to higher observed NO_2 surface concentrations. The changes due to the inclusion of either the MODIS LAI or the updated z_0 values in our model are limited.

Both Table S1, Table S2 and Figure 16 illustrate that the comparability of the modelled wet deposition and surface concentration fields to the available in-situ measurements did not change significantly. The impact of the updated LAI and z_0 values on these fields is largely an indirect effect of the more distinct changes in the dry deposition, and thus too small to lead to any drastic changes. We conclude that we are unable to demonstrate any major improvements with the use of the currently available in-situ measurements.

5. Discussion

This paper aimed to improve the surface characterization of LOTOS-EUROS through the inclusion of satellite-derived leaf area index (LAI) and roughness length (z_0) values. We used empirical functions to derive roughness length (z_0) values for different land use classes. The updated z_0 values are compared to literature values, showing a good agreement in general. We also compared the z_0 values to z_0 values computed from FLUXNET sites. The z_0 values for forest seemed to match well. The z_0 values for short vegetation seem to be overestimated for crops and underestimated for grassland and wetland sites. The differences for short vegetation types can be partially explained by the large inter-site variability in vegetation types within each classified land use (e.g. reeds versus short grass). The equation used for grassland in this study seems to work best for short grasslands. For our current study area, this does not pose a problem, since most grasslands in Germany, Belgium and the Netherlands are managed and grazed upon. We found an improved RMSD value of 0.60, compared to RMDS of 0.76 with default z_0 values. Even though there is an offset between the satellite-derived and computed FLUXNET z_0 values for crops, the seasonal pattern seemed to match well. The offset can be explained by the absence of low NDVI (<0.4) values.

The z_0 is closely related to the geometric features and distributions of the roughness elements in a certain area. The updated z_0 values are linked to specific land use pixels and are therefore assumed reasonable estimates for moderately homogeneous areas with this specific land use type. There are various approaches to combine these z_0 values into an ‘effective’ roughness for larger, mixed areas (e.g. (Claussen, 1990;Mason, 1988)). The LOTOS-

EUROS model uses logarithmic averaging to compute an effective roughness for an entire model pixel. This averaging step seems to be one of the reasons why the effect of our updated z_0 values on the deposition fields is limited. To illustrate this, the relative change in total dry NH_3 deposition due to the updated z_0 values were computed and shown in Figure 17. We used increasing threshold percentages to sort the NH_3 deposition on a model pixel level per land use type and fraction. Figure 17 shows that the differences in total NH_3 deposition between the two runs increase with increasing land use fraction. The model pixels that mostly consist of one type of land use seem to show the largest change in NH_3 deposition. The change thus appears to be less distinct in pixels that have a higher degree of mixing. Most of the model pixels largely contain mixtures of different land uses on the current model resolution. As a result, averaging of z_0 on a model pixel level is thus likely to cause a levelling effect on the current model resolution. The impact of the updated z_0 values is therefore expected to be larger at a higher model resolution. The use of another approach for computing the 'effective' roughness could potentially lead to stronger changes in the modelled deposition fields.

Moreover, we should also consider the limitations of the datasets used in this study. The forest canopy height map used in this study has been validated against 66 FLUXNET sites (Simard et al., 2011). The results showed that RMSE = 4.4 m and R^2 = 0.7 after removal of 7 outliers. For the FLUXNET forest sites used in this study, we compared the forest canopy heights from GLAS to the maximum forest canopy height at the FLUXNET sites taken from (Flechard et al., 2019). For all but one site (DE-Hai), the forest canopy heights from GLAS were lower than this value (Table S3). This method could potentially be improved by using another product with either a higher precision or resolution. For modelling studies on a national level one could or instance consider the use of airborne LiDAR point clouds to retrieve forest canopy heights. This procedure, although it is computationally expensive, would allow us to create high resolution z_0 maps.

The MODIS-LAI at the FLUXNET sites showed realistic seasonal variations for most land use classifications, except for relatively low winter-time values for evergreen needle leaf forests. The previous versions of the MODIS-LAI have been validated in many studies (e.g. (Fang et al., 2012;Wang et al., 2004;Kobayashi et al., 2010)), showing an overall good agreement with ground observed LAI values and other LAI products. The seasonality in LAI is properly captured for most biomes, but unrealistic temporal variability is observed for forest due to infrequent observations. Also, the previous versions overestimate LAI for forests (Fang et al., 2012;Kobayashi et al., 2010;Wang et al., 2004). The MODIS-LAI products have been gradually improving with each update, however, these issues still exist in the newer versions of the product. For the most recent version of the MODIS-LAI, version 6, Yan et al. (2016) found an overall RMSE of 0.66 and a R^2 of 0.77 in comparison with LAI ground observation. More recently, using a different approach, Xu et al. (2018) found a slightly higher RMSE of 0.93 and a R^2 of 0.77. Some studies (e.g. Tian et al., 2004) have reported an underestimation of the MODIS-LAI in presence of snow-cover, particularly affecting evergreen forests. There was only a limited amount of snowfall in our study region, so this did not lead to any problems. However, this issue should be carefully considered when using the MODIS-LAI for regions with frequent snow-cover, like Scandinavia. LOTOS-EUROS uses meteorological data to determine what regions are covered with snow. If a certain location is snow-covered, the standard parameterization for the

canopy resistance is not used. LOTOS-EUROS uses a pre-defined value for the canopy resistance instead. As such, these low MODIS-LAI values do not affect the modelled deposition in LOTOS-EUROS during snow-cover.

Though the issues with the MODIS-LAI should be considered with care, the spatial and temporal distribution of these LAI values is more realistic than that of the default LAI values used in LOTOS-EUROS. The same holds for the updated, time-variant z_0 values. The representation of the growing season is now more realistic due to their dependence on NDVI and LAI values. Moreover, the z_0 values for forests now also have a clear spatial variation, such as a latitudinal gradient with increasing z_0 values towards the south of Germany. These type of patterns can simply not be captured by fixed values.

We evaluated the effect of updated z_0 and LAI values on modelled N_r distribution and deposition fields. The distribution of the relative changes in deposition of the reduced and oxidized forms of reactive nitrogen showed a similar pattern. Here, the updated z_0 values led to a variation of ~±8%, and the updated LAI values led to variations of ~±30% in both fields. The dry deposition fields were most sensitive to changes in z_0 and LAI, as these varied from approximately -20% to +20% with the updated z_0 map, and from -20% even up to +30% with the MODIS LAI values. As a result, we observed a shift from wet to dry deposition, except for the Netherlands, where we observe an opposite shift, from dry to wet deposition. Moreover, we observed a redistribution of N_r deposition over different land use classes on a sub grid level. To illustrate the potential consequences on a local scale, we computed the critical load exceedances for deciduous and coniferous forest (Figure 18) using critical loads of 10 kg following Bobbink et al. (2010b). Compared to the default run, the changes may be sizable locally, ranging from approximately -3 kg up to +2 kg for deciduous forest and even over -3 kg for coniferous forest.

The uncertainties of the LAI and z_0 input data are but one aspect of the model uncertainty of CTMs. The model uncertainty has several other origins, like the physical parameterizations (e.g. deposition velocities) and the numerical approximations (e.g. grid size). Two of the most important uncertainties related to deposition modelling are the emissions and the surface exchange parameterization. The emission inventories for reactive nitrogen hold a relatively large uncertainty. The uncertainty of the reported annual total NH_3 emissions is estimated to be at least ±30%. This is mainly due to the diverse nature of agricultural emission sources, leading to large spatio-temporal variations. The annual NO_x emissions total hold a lower uncertainty, of approximately ±20% (Kuenen et al., 2014). Emissions at specific locations, especially for NH_3, are even more uncertain due to assumptions made in the redistribution and timing of emissions. A recent paper of Dammers et al., 2019, for instance, found that satellite-derived NH_3 emissions of large point sources are a factor 2.5 higher than those given in emission N-inventories. The surface-exchange parameterization is another source of uncertainty. The complexity of the NH_3 surface exchange schemes in CTMs is usually low compared to the current level of process understanding (Flechard et al., 2013). Moreover, large discrepancies exist between deposition schemes. Flechard et al. (2011) for instance showed that the differences between four dry deposition schemes for reactive nitrogen can be as large as a factor 2-3.

This work has shown that changes in two of the main deposition parameters (LAI, z_0) can already lead to distinct, systematic changes (~30%) in the modelled deposition fields. This demonstrates the model's sensitivity toward these

input values, especially the LAI. In addition to the known uncertainty involved with surface exchange parameterization itself, this further stresses the need for further research. Another important aspect that should receive more attention is the validation of the dry deposition fields with in-situ dry deposition measurements. Here we illustrated the need for direct validation methods, as relatively large changes in modelled dry deposition field cannot be verified sufficiently by surface concentration and wet deposition measurements.

The surface-atmosphere exchange remains one of the most important uncertainties in deposition modelling. The use of satellite products to derive LAI and z_0 values can help us to represent the surface characterization in models more accurately, which in turn might help us to minimize the uncertainty in deposition modelling. The approach to derive high resolution, dynamic z_0 estimates presented here can be linked to any land use map and is as such transferable to many different models and geographical areas.

Data availability. LOTOS-EUROS v2.0 is available for download under license at https://lotos-euros.tno.nl/. The adjusted model routines to read in the z_0 and LAI values are available in cooperation with TNO and can be disclosed upon request. All MODIS products used in this study are open-source and can be downloaded at https://ladsweb.nascom.nasa.gov. The global forest canopy height dataset can be downloaded at https://daac.ornl.gov/. The population density grid can be downloaded at https://www.eea.europa.eu/.

Acknowledgements. We would like to thank the Umweltbundesamt (UBA), the German monitoring networks, as well as the European Monitoring and Evaluation Programme (EMEP) and the Rijksinstituut voor Volksgezondheid en Milieu (RIVM) for providing the in-situ observations used for validation. This work used eddy covariance data acquired and shared by the FLUXNET community, including these networks: AmeriFlux, AfriFlux, AsiaFlux, CarboAfrica, CarboEuropeIP, CarboItaly, CarboMont, ChinaFlux, Fluxnet-Canada, GreenGrass, ICOS, KoFlux, LBA, NECC, OzFlux-TERN, TCOS-Siberia, and USCCC. The ERA-Interim reanalysis data are provided by ECMWF and processed by LSCE. The FLUXNET eddy covariance data processing and harmonization was carried out by the European Fluxes Database Cluster, AmeriFlux Management Project, and Fluxdata project of FLUXNET, with the support of CDIAC and ICOS Ecosystem Thematic Center, and the OzFlux, ChinaFlux and AsiaFlux offices.

Author Contribution. JWE, MS and SG designed the research. RK, AS and SG performed the model simulations. SG did the input data processing and model output analysis. All authors contributed to the interpretation of the results. SG wrote the paper with contributions from all co-authors.

Competing interests. The authors declare that they have no conflict of interest.

References

Abida, R., Attié, J.-L., El Amraoui, L., Lahoz, W. A., Ricaud, P., Eskes, H., Segers, A., Curier, L., de Haan, J., and Kujanpää, J.: Impact of spaceborne carbon monoxide observations from the S-5P platform on tropospheric composition analyses and forecasts, 2017.

Banzhaf, S., Schaap, M., Kerschbaumer, A., Reimer, E., Stern, R., Van Der Swaluw, E., & Builtjes, P. Implementation and evaluation of pH-dependent cloud chemistry and wet deposition in the chemical transport model REM-Calgrid. Atmospheric environment, 49, 378-390, 2012.

Bauer, S. E., Tsigaridis, K., and Miller, R.: Significant atmospheric aerosol pollution caused by world food cultivation, Geophys Res Lett, 43, 5394-5400, 2016.

Behera, S. N., Sharma, M., Aneja, V. P., and Balasubramanian, R.: Ammonia in the atmosphere: a review on emission sources, atmospheric chemistry and deposition on terrestrial bodies, Environmental Science and Pollution Research, 20, 8092-8131, 2013..

Bobbink, R., Hicks, K., Galloway, J., Spranger, T., Alkemade, R., Ashmore, M., Bustamante, M., Cinderby, S., Davidson, E., and Dentener, F.: Global assessment of nitrogen deposition effects on terrestrial plant diversity: a synthesis, Ecol Appl, 20, 30-59, 2010a.

Bobbink, R., Hicks, K., Galloway, J., Spranger, T., Alkemade, R., Ashmore, M., Bustamante, M., Cinderby, S., Davidson, E., Dentener, F., Emmett, B., Erisman, J. W., Fenn, M., Gilliam, F., Nordin, A., Pardo, L., and De Vries, W.: Global assessment of nitrogen deposition effects on terrestrial plant diversity: a synthesis, Ecol Appl, 20, 30-59, Doi 10.1890/08-1140.1, 2010b.

Bolle, H., and Streckenbach, B.: Flux estimates from remote sensing, The Echival Field Experiment in a Desertification Threatened Area (EFEDA), final report, 406-424, 1993.

Brutsaert, W.: Evaporation into the atmosphere: theory, history and applications, Springer Science & Business Media, 2013.

Businger, J. A., Wyngaard, J. C., Izumi, Y., and Bradley, E. F.: Flux-profile relationships in the atmospheric surface layer, Journal of the atmospheric Sciences, 28, 181-189, 1971.

Butterbach-Bahl, K., Nemitz, E., Zaehle, S., Billen, G., Boeckx, P., Erisman, J. W., Garnier, J., Upstill-Goddard, R., Kreuzer, M., and Oenema, O.: Nitrogen as a threat to the European greenhouse balance, 2011.

Chen, Q., Jia, L., Hutjes, R., and Menenti, M. Estimation of aerodynamic roughness length over oasis in the Heihe River Basin by utilizing remote sensing and ground data. Remote Sensing, 7(4), 3690-3709, 2015.

Claussen, M.: Area-averaging of surface fluxes in a neutrally stratified, horizontally inhomogeneous atmospheric boundary-layer, Atmos Environ a-Gen, 24, 1349-1360, 1990.

Colette, A., Andersson, C., Manders, A., Mar, K., Mircea, M., Pay, M., Raffort, V., Tsyro, S., Cuvelier, C., and Adani, M.: EURODELTA-Trends, a multi-model experiment of air quality hindcast in Europe over 1990–2010, Geosci. Model Dev., 10, 3255–3276. 2017.

Curier, R., Kranenburg, R., Segers, A., Timmermans, R., and Schaap, M.: Synergistic use of OMI NO2 tropospheric columns and LOTOS–EUROS to evaluate the NOx emission trends across Europe, Remote Sens Environ, 149, 58-69, 2014.

Dammers, E., McLinden, C. A., Griffin, D., Shephard, M. W., Van Der Graaf, S., Lutsch, E., Schaap, M., Gainairu-Matz, Y., Fioletov, V., Van Damme, M., Whitburn, S., Clarisse, L., Cady-Pereira, K., Clerbaux, C., Coheur, P. F., and Erisman, J. W.: NH3 emissions from large point sources derived from CrIS and IASI satellite observations, Atmos. Chem. Phys., 19, 12261–12293, https://doi.org/10.5194/acp-19-12261-2019, 2019.

Davi, H., Soudani, K., Deckx, T., Dufrene, E., Le Dantec, V., and Francois, C.: Estimation of forest leaf area index from SPOT imagery using NDVI distribution over forest stands, Int J Remote Sens, 27, 885-902, 2006.

Didan, K.: MYD13A3 MODIS/Aqua Vegetation Indices Monthly L3 Global 1km SIN Grid V006, NASA EOSDIS LP DAAC, 10.5067/MODIS/MYD13A3.006, 2015.

Emberson, L., Simpson, D., Tuovinen, J., Ashmore, M., and Cambridge, H.: Towards a model of ozone deposition and stomatal uptake over Europe, EMEP MSC-W Note, 6, 1-57, 2000.

EMEP: The European Monitoring and Evaluation Programme EMEP Status Report, 2016.

Erisman, J., and Schaap, M.: The need for ammonia abatement with respect to secondary PM reductions in Europe, Environ Pollut, 129, 159-163, 2004.

Erisman, J. W., and Duyzer, J. A micrometeorological investigation of surface exchange parameters over heathland. Boundary-layer meteorology, 57(1-2), 115-128, 1991.

Erisman, J. W., Van Pul, A., and Wyers, P.: Parametrization of surface resistance for the quantification of atmospheric deposition of acidifying pollutants and ozone, Atmos Environ, 28, 2595-2607, 1994.

Erisman, J. W., Galloway, J., Seitzinger, S., Bleeker, A., and Butterbach-Bahl, K.: Reactive nitrogen in the environment and its effect on climate change, Curr Opin Env Sust, 3, 281-290, 2011.

European Centre for Medium-Range Weather Forecasts: Annual report, 2016.

European Environmental Agency: CLC2012 Addendum to CLC2006 Technical Guidelines, EEA Report, 2014.

European Environmental Agency: Airbase dataset, http://discomap.eea.europa.eu, 2019.

Fang, H., Wei, S., and Liang, S.: Validation of MODIS and CYCLOPES LAI products using global field measurement data, Remote Sens Environ, 119, 43-54, 2012.

Flechard, C. R., Nemitz, E., Smith, R. I., Fowler, D., Vermeulen, A. T., Bleeker, A., Erisman, J. W., Simpson, D., Zhang, L., Tang, Y. S., and Sutton, M. A.: Dry deposition of reactive nitrogen to European ecosystems: a comparison of inferential models across the NitroEurope network, Atmos. Chem. Phys., 11, 2703–2728, https://doi.org/10.5194/acp-11-2703-2011, 2011.

Flechard, C., Massad, R.-S., Loubet, B., Personne, E., Simpson, D., Bash, J., Cooter, E., Nemitz, E., and Sutton, M.: Advances in understanding, models and parameterizations of biosphere-atmosphere ammonia exchange, in: Review and Integration of Biosphere-Atmosphere Modelling of Reactive Trace Gases and Volatile Aerosols, Springer, 11-84, 2013.

Flechard, C. R., Ibrom, A., Skiba, U. M., de Vries, W., van Oijen, M., Cameron, D. R., Dise, N. B., Korhonen, J. F. J., Buchmann, N., Legout, A., Simpson, D., Sanz, M. J., Aubinet, M., Loustau, D., Montagnani, L., Neirynck, J., Janssens, I. A., Pihlatie, M., Kiese, R., Siemens, J., Francez, A.-J., Augustin, J., Varlagin, A., Olejnik, J., Juszczak, R., Aurela, M., Chojnicki, B. H., Dämmgen, U., Djuricic, V., Drewer, J., Eugster, W., Fauvel, Y., Fowler, D., Frumau, A., Granier, A., Gross, P., Hamon, Y., Helfter, C., Hensen, A., Horváth, L., Kitzler, B., Kruijt, B., Kutsch, W. L., Lobo-do-Vale, R., Lohila, A., Longdoz, B., Marek, M. V., Matteucci, G., Mitosinkova, M., Moreaux, V., Neftel, A., Ourcival, J.-M., Pilegaard, K., Pita, G., Sanz, F., Schjoerring, J. K., Sebastià, M.-T., Tang, Y. S., Uggerud, H., Urbaniak, M., van Dijk, N., Vesala, T., Vidic, S., Vincke, C., Weidinger, T., Zechmeister-Boltenstern, S., Butterbach-Bahl, K., Nemitz, E., and Sutton, M. A.: Carbon / nitrogen interactions in European forests and semi-natural vegetation. Part I: Fluxes and budgets of carbon, nitrogen and greenhouse gases from ecosystem monitoring and modelling, Biogeosciences Discuss., https://doi.org/10.5194/bg-2019-333, in review, 2019.

Fowler, D., Steadman, C. E., Stevenson, D., Coyle, M., Rees, R. M., Skiba, U., Sutton, M., Cape, J., Dore, A., and Vieno, M.: Effects of global change during the 21st century on the nitrogen cycle, Atmos Chem Phys, 15, 13849-13893, 2015.

Gallagher, M., Nemitz, E., Dorsey, J., Fowler, D., Sutton, M., Flynn, M., and Duyzer, J.: Measurements and parameterizations of small aerosol deposition velocities to grassland, arable crops, and forest: Influence of surface roughness length on deposition, Journal of Geophysical Research: Atmospheres, 107, 2002.

Gallego, F. J.: A population density grid of the European Union, Population and Environment, 31, 460-473, 2010.

Galloway, J. N., Aber, J. D., Erisman, J. W., Seitzinger, S. P., Howarth, R. W., Cowling, E. B., and Cosby, B. J.: The nitrogen cascade, AIBS Bulletin, 53, 341-356, 2003.

Galloway, J. N., Dentener, F. J., Capone, D. G., Boyer, E. W., Howarth, R. W., Seitzinger, S. P., Asner, G. P., Cleveland, C. C., Green, P., and Holland, E. A.: Nitrogen cycles: past, present, and future, Biogeochemistry, 70, 153-226, 2004.

Galloway, J. N., Townsend, A. R., Erisman, J. W., Bekunda, M., Cai, Z. C., Freney, J. R., Martinelli, L. A., Seitzinger, S. P., and Sutton, M. A.: Transformation of the nitrogen cycle: Recent trends, questions, and potential solutions, Science, 320, 889-892, 10.1126/science.1136674, 2008.

Graf, A., van de Boer, A., Moene, A., and Vereecken, H. Intercomparison of methods for the simultaneous estimation of zero-plane displacement and aerodynamic roughness length from single-level eddy-covariance data. Boundary-layer meteorology, 151(2), 373-387, 2014.

Hatfield, J.: Large scale evapotranspiration from remotely sensed surface temperature, Planning Now for Irrigation and Drainage in the 21st Century, 1988, 502-509,

Hendriks, C., Kranenburg, R., Kuenen, J. J. P., Van den Bril, B., Verguts, V., and Schaap, M.: Ammonia emission time profiles based on manure transport data improve ammonia modelling across north western Europe, Atmos Environ, 131, 83-96, 10.1016/j.atmosenv.2016.01.043, 2016.

Houborg, R., and Boegh, E.: Mapping leaf chlorophyll and leaf area index using inverse and forward canopy reflectance modeling and SPOT reflectance data, Remote Sens Environ, 112, 186-202, 2008.

Jonckheere, I., Fleck, S., Nackaerts, K., Muys, B., Coppin, P., Weiss, M., and Baret, F.: Review of methods for in situ leaf area index determination: Part I. Theories, sensors and hemispherical photography, Agr Forest Meteorol, 121, 19-35, 2004.

Kobayashi, H., Delbart, N., Suzuki, R., and Kushida, K.: A satellite-based method for monitoring seasonality in the overstory leaf area index of Siberian larch forest, Journal of Geophysical Research: Biogeosciences, 115, 2010.

Kuenen, J. J. P., Visschedijk, A. J. H., Jozwicka, M., and van der Gon, H. A. C. D.: TNO-MACC_II emission inventory; a multi-year (2003-2009) consistent high-resolution European emission inventory for air quality modelling, Atmos Chem Phys, 14, 10963-10976, 10.5194/acp-14-10963-2014, 2014.

Lankreijer, H., Hendriks, M., and Klaassen, W.: A comparison of models simulating rainfall interception of forests, Agr Forest Meteorol, 64, 187-199, 1993.

Lelieveld, J., Evans, J. S., Fnais, M., Giannadaki, D., and Pozzer, A.: The contribution of outdoor air pollution sources to premature mortality on a global scale, Nature, 525, 367, 2015.

Lolkema, D. E., Noordijk, H., Stolk, A. P., Hoogerbrugge, R., van Zanten, M. C., and van Pul, W. A. J.: The Measuring Ammonia in Nature (MAN) network in the Netherlands, Biogeosciences, 12, 5133-5142, 10.5194/bg-12-5133-2015, 2015.

Mailler, S., Menut, L., Khvorostyanov, D., Valari, M., Couvidat, F., Siour, G., Turquety, S., Briant, R., Tuccella, P., and Bessagnet, B.: CHIMERE-2017: from urban to hemispheric chemistry-transport modeling, Geosci Model Dev, 10, 2397-2423, 2017.

Manders-Groot, A., Segers, A., Jonkers, S., Schaap, M., Timmermans, R., Hendriks, C., Sauter, F., Kruit, R. W., van der Swaluw, E., and Eskes, H.: LOTOS-EUROS v2. 0 reference guide, TNO report TNO2016, 10898, 2016.

Manders, A. M. M., Builtjes, P. J. H., Curier, L., Denier van der Gon, H. A. C., Hendriks, C., Jonkers, S., Kranenburg, R., Kuenen, J., Segers, A. J., Timmermans, R. M. A., Visschedijk, A., Wichink Kruit, R. J., Van Pul, W. A. J., Sauter, F. J., van der Swaluw, E., Swart, D. P. J., Douros, J., Eskes, H., van Meijgaard, E., van Ulft, B., van Velthoven, P., Banzhaf, S., Mues, A., Stern, R., Fu, G., Lu, S., Heemink, A., van Velzen, N., and Schaap, M.: Curriculum vitae of the LOTOS–EUROS (v2.0) chemistry transport model, Geosci Model Dev, 10(11), 10.5194/gmd-10-4145-2017, 2017.

Maurer, K.D., Hardiman, B.S., Vogel, C.S. and Bohrer, G. Canopy-structure effects on surface roughness parameters: Observations in a Great Lakes mixed-deciduous forest. Agric. For. Meteorol, 177, 24–34, 2013.

Mason, P.: The formation of areally-averaged roughness lengths, Q J Roy Meteor Soc, 114, 399-420, 1988.

McNaughton, K. G., and Van Den Hurk, B. J. J. M.: A 'Lagrangian' revision of the resistors in the two-layer model for calculating the energy budget of a plant canopy, Bound-Lay Meteorol, 74, 261-288, 10.1007/bf00712121, 1995.

Moran, M. S.: A satellite-based approach for evaluation of the spatial distribution of evapotranspiration from agricultural lands, 1990.

Myneni, R., Knyazikhin, Y., and Park, T.: MCD15A2H MODIS/Terra+Aqua Leaf Area Index/FPAR 8-day L4 Global 500m SIN Grid V006, NASA EOSDIS Land Processes DAAC, 10.5067/MODIS/MCD15A2H.006, 2015.

Nakai, T.: Parameterisation of aerodynamic roughness over boreal, cool-and warm-temperate forests, Agr Forest Meteorol, 148, 1916, 2008.

Paerl, H. W., Gardner, W. S., McCarthy, M. J., Peierls, B. L., and Wilhelm, S. W.: Algal blooms: noteworthy nitrogen, Science, 346, 175-175, 2014.

Pastorello, G. Z., Papale, D., Chu, H., Trotta, C., Agarwal, D., Canfora, E., Baldocchi, D. and Torn, M. The FLUXNET2015 dataset: The longest record of global carbon, water, and energy fluxes is updated. Eos, 98, 2017.

Plate, E. J.: Aerodynamic Characteristics of Atmospheric Boundary Layers, Argonne National Lab., Ill. Karlsruhe Univ.(West Germany), 1971.

Raupach, M.: Simplified expressions for vegetation roughness length and zero-plane displacement as functions of canopy height and area index, Bound-Lay Meteorol, 71, 211-216, 1994.

Reis, S., Pinder, R., Zhang, M., Lijie, G., and Sutton, M.: Reactive nitrogen in atmospheric emission inventories, Atmos Chem Phys, 9, 7657-7677, 2009.

Schaap, M., Manders, A., Hendricks, J. M., Cnossen, A. J. S., Segers, H. A. C., Denier van der Gon, M., Jozwicka, M., Sauter, F., Velders, G., Matthijsen, J., and Builtjes, P.: Regional modelling of particulate matter for the Netherlands, Netherlands Research Program on Particulate Matter, 500099008, 2009.

Schaap, M., Banzhaf, S., Scheuschner, T., Geupel, M., Hendriks, C., Kranenburg, R. and Builtjes, P. J. H. : Atmospheric nitrogen deposition to terrestrial ecosystems across Germany, Biogeosciences, in review, 2019.

Schaudt, K., and Dickinson, R.: An approach to deriving roughness length and zero-plane displacement height from satellite data, prototyped with BOREAS data, Agr Forest Meteorol, 104, 143-155, 2000.

Schrader, F., and Brummer, C.: Land Use Specific Ammonia Deposition Velocities: a Review of Recent Studies (2004-2013), Water Air Soil Poll, 225, ARTN 2114 10.1007/s11270-014-2114-7, 2014.

Schrader, F., Brummer, C., Flechard, C. R., Kruit, R. J. W., van Zanten, M. C., Zoll, U., Hensen, A., and Erisman, J. W.: Non-stomatal exchange in ammonia dry deposition models: comparison of two state-of-the-art approaches, Atmos Chem Phys, 16, 13417-13430, 10.5194/acp-16-13417-2016, 2016.

Silva, J., Ribeiro, C., and Guedes, R.: Roughness length classification of Corine Land Cover classes, Proceedings of the European Wind Energy Conference, Milan, Italy, 2007, 110,

Simard, M., Pinto, N., Fisher, J. B., and Baccini, A.: Mapping forest canopy height globally with spaceborne lidar, Journal of Geophysical Research: Biogeosciences, 116, 2011.

Simpson, D., Benedictow, A., Berge, H., Bergström, R., Emberson, L. D., Fagerli, H., Flechard, C. R., Hayman, G. D., Gauss, M., Jonson, J. E., Jenkin, M. E., Nyíri, A., Richter, C., Semeena, V. S., Tsyro, S., Tuovinen, J. P., Valdebenito, Á., and Wind, P.: The EMEP MSC-W chemical transport model – technical description, Atmos. Chem. Phys., 12, 7825-7865, 10.5194/acp-12-7825-2012, 2012.

Skjøth, C. A., Geels, C., Berge, H., Gyldenkærne, S., Fagerli, H., Ellermann, T., Frohn, L. M., Christensen, J., Hansen, K. M., Hansen, K., and Hertel, O.: Spatial and temporal variation in ammonia emissions - a freely accessible model code for Europe Atmos Chem Phys, 11, 5221-5236, 10.5194/acp-11-5221-2011, 2011.

Soudani, K., François, C., Le Maire, G., Le Dantec, V., and Dufrêne, E.: Comparative analysis of IKONOS, SPOT, and ETM+ data for leaf area index estimation in temperate coniferous and deciduous forest stands, Remote Sens Environ, 102, 161-175, 2006.

Tian, Y., Dickinson, R. E., Zhou, L., Zeng, X., Dai, Y., Myneni, R. B., ... & Wu, W. Comparison of seasonal and spatial variations of leaf area index and fraction of absorbed photosynthetically active radiation from Moderate Resolution Imaging Spectroradiometer (MODIS) and Common Land Model. Journal of Geophysical Research: Atmospheres, 109(D1), 2004.

Troen, I., and Petersen, E. L.: European wind atlas. Risø national laboratory, Roskilde, Weibull W.(1951). A statistical distribution function of wide applicability. J. Appl. mech, 18, 293-297, 1989.

Turner, D. P., Cohen, W. B., Kennedy, R. E., Fassnacht, K. S., and Briggs, J. M.: Relationships between leaf area index and Landsat TM spectral vegetation indices across three temperate zone sites, Remote Sens Environ, 70, 52-68, 1999.

Van Zanten, M., Kruit, R. W., Hoogerbrugge, R., Van der Swaluw, E., and Van Pul, W.: Trends in ammonia measurements in the Netherlands over the period 1993–2014, Atmos Environ, 148, 352-360, 2017.

van Zanten, M. C., Sauter, F. J., Wichink Kruit, R. J., van Jaarsveld, J. A., and van Pul, M. A. J.: Description of the DEPAC module: Dry deposition modelling with DEPAC_GCN2010, Rivm Report 680180001/2010, RIVM, Bilthoven, Netherlands, 2010.

Wang, Y., Woodcock, C. E., Buermann, W., Stenberg, P., Voipio, P., Smolander, H., Häme, T., Tian, Y., Hu, J., and Knyazikhin, Y.: Evaluation of the MODIS LAI algorithm at a coniferous forest site in Finland, Remote Sens Environ, 91, 114-127, 2004.

Watson, D. J.: Comparative physiological studies on the growth of field crops: I. Variation in net assimilation rate and leaf area between species and varieties, and within and between years, Annals of botany, 11, 41-76, 1947.

Wesely, M.: Parameterization of surface resistances to gaseous dry deposition in regional-scale numerical models, Atmospheric Environment (1967), 23, 1293-1304, 1989.

Wichink Kruit, R. J., Schaap, M., Sauter, F. J., van Zanten, M. C., and van Pul, W. A. J.: Modeling the distribution of ammonia across Europe including bi-directional surface-atmosphere exchange, Biogeosciences, 9, 5261-5277, 10.5194/bg-9-5261-2012, 2012.

Wieringa, J.: Representative roughness parameters for homogeneous terrain, Bound-Lay Meteorol, 63, 323-363, 1993.

Wu, Z., Schwede, D. B., Vet, R., Walker, J. T., Shaw, M., Staebler, R., and Zhang, L.: Evaluation and intercomparison of five North American dry deposition algorithms at a mixed forest site, Journal of Advances in Modeling Earth Systems, 10, 1571-1586, 2018.

Xing, Q., Wu, B., Yan, N., Yu, M., and Zhu, W.: Evaluating the relationship between field aerodynamic roughness and the MODIS BRDF, NDVI, and wind speed over grassland, Atmosphere, 8, 16, 2017.

Xu, B., Li, J., Park, T., Liu, Q., Zeng, Y., Yin, G., Zhao, J., Fan, W., Yang, L., and Knyazikhin, Y.: An integrated method for validating long-term leaf area index products using global networks of site-based measurements, Remote Sens Environ, 209, 134-151, 2018.

Yan, K., Park, T., Yan, G., Liu, Z., Yang, B., Chen, C., Nemani, R. R., Knyazikhin, Y., and Myneni, R. B.: Evaluation of MODIS LAI/FPAR product collection 6. Part 2: Validation and intercomparison, Remote Sensing, 8, 460, 2016.

Yang, R., and Friedl, M. A.: Determination of roughness lengths for heat and momentum over boreal forests, Bound-Lay Meteorol, 107, 581-603, 2003.

Yu, M., Wu, B., Yan, N., Xing, Q., and Zhu, W.: A method for estimating the aerodynamic roughness length with NDVI and BRDF signatures using multi-temporal Proba-V data, Remote Sensing, 9, 6, 2016.

Zwally, H., Schutz, B., Abdalati, W., Abshire, J., Bentley, C., Brenner, A., Bufton, J., Dezio, J., Hancock, D., and Harding, D.: ICESat's laser measurements of polar ice, atmosphere, ocean, and land, Journal of Geodynamics, 34, 405-445, 2002.

Table 1: Overview of eddy-covariance sites used to compute z_0. The following abbreviations for land use types are used: DBF - Deciduous broadleaf forest, ENF - Evergreen needle leaf coniferous forest, MF - Mixed forest, CRO – Croplands, WET – Permanent wetlands, GRA – Grasslands

Site ID	Site name	Latitude	Longitude	Land use	z (m)	FLUXNET2015 DOI
BE-Bra	Brasschaat	51.30761	4.51984	MF	41.0	10.18140/FLX/1440128
BE-Lon	Lonzee	50.5516	4.74613	CRO	2.7	10.18140/FLX/1440129
BE-Vie	Vielsalm	50.30496	5.99808	MF	51.0	10.18140/FLX/1440130
DE-Akm	Anklam	53.86617	13.68342	WET	9.5	10.18140/FLX/1440213
DE-Geb	Gebesee	51.1001	10.9143	CRO	3.5	10.18140/FLX/1440146
DE-Gri	Grillenburg	50.95004	13.51259	GRA	3.0	10.18140/FLX/1440147
DE-Hai (2012)	Hainich	51.07917	10.4530	DBF	42.0	10.18140/FLX/1440148
DE-Kli	Klingenberg	50.89306	13.52238	CRO	3.5	10.18140/FLX/1440149
DE-Obe	Oberbärenburg	50.78666	13.72129	ENF	30.0	10.18140/FLX/1440151
DE-RuR	Rollesbroich	50.62191	6.30413	GRA	2.6	10.18140/FLX/1440215
DE-RuS	Selhausen Juelich	50.86591	6.44717	CRO	2.5	10.18140/FLX/1440216
DE-Seh (2010)	Selhausen	50.87062	6.44965	CRO	2.0	10.18140/FLX/1440217
DE-SfN	Schechenfilz Nord	47.80639	11.3275	WET	6.7	10.18140/FLX/1440219
DE-Tha	Tharandt	50.96235	13.56516	ENF	42.0	10.18140/FLX/1440152
NL-Hor (2011)	Horstermeer	52.24035	5.0713	GRA	4.3	10.18140/FLX/1440177
NL-Loo (2013)	Loobos	52.16658	5.74356	ENF	26	10.18140/FLX/1440178
FR-Fon	Fontainebleau-Barbeau	48.47636	2.7801	DBF	37	10.18140/FLX/1440161
CH-Cha	Chamau	47.21022	8.41044	GRA	2.4	10.18140/FLX/1440131
CH-Fru	Früebüel	47.11583	8.53778	GRA	2.5	10.18140/FLX/1440133
CH-Lae	Laegern	47.47808	8.3650	MF	47	10.18140/FLX/1440134
CH-Oe1 (2008)	Oensingen grassland	47.28583	7.73194	GRA	1.2	10.18140/FLX/1440135
CH-Oe2	Oensingen crop	47.28631	7.73433	CRO	2.25	10.18140/FLX/1440136
CZ-wet	Trebon	49.02465	14.77035	WET	2.6	10.18140/FLX/1440145

Table 2: An overview of the datasets that are used to derive z_0 input values for each DEPAC land use category.

DEPAC class	Dataset
1 - Grass	MODIS NDVI
2 - Arable land	MODIS NDVI
3 - Permanent crops	MODIS NDVI
4 - Coniferous forest	GLAS forest canopy height
5 - Deciduous forest	GLAS forest canopy height, MODIS LAI
6 - Water	-
7 - Urban	Population density
8 - Other	MODIS NDVI
9 - Desert	-

Table 3: Studies that relate the aerodynamic roughness length (z_0) to satellite-derived NDVI values for specific land cover types and conditions.

Function		Vegetation type(s)	Reference
$z_0 = \begin{cases} -0.173 + 1.168 * NDVI - 1.125 * NDVI^2 & \text{for } NDVI < 0.6 \\ 0.1 & \text{for } NDVI \geq 0.6 \end{cases}$	(eq. 6)	Partial cover cotton and wheat canopies	Hatfield (1988)
$z_0 = e^{-5.2+5.3*NDVI}$	(eq. 7)	Alfalfa (Arizona)	Moran (1990)
$z_0 = e^{-5.5+5.8*NDVI}$	(eq. 8)	Mixed, non-irrigated agricultural land (Mediterranean)	Bolle and Streckenbach (1993)
$z_0 = 0.2255 * NDVI + 0.0087$	(eq. 9)	Spring maize	Yu et al. (2016)
$z_0 = 0.2476 * NDVI + 0.0615$	(eq. 10)	Winter wheat	Yu et al. (2016)
$z_0 = 0.2858 * NDVI + 0.1017$	(eq. 11)	Summer maize	Yu et al. (2016)
$z_0 = 0.0203 * NDVI^{0.9547}$	(eq. 12)	Grassland	Xing et al. (2017)

Table 4: An overview of the default and the adjusted roughness length of each DEPAC class used in LOTOS-EUROS for Germany, the Netherlands and Belgium. The datasets that are used to derive the updated z_0 values are given in the last column. The mean z_0 value of the DEPAC classes computed using the MODIS NDVI product is the yearly mean of all monthly z_0 values.

DEPAC class	**Default z_0**	**New mean z_0 (σ)**
1 - Grass	0.03	0.013 (0.002)
2 - Arable land	0.1	0.19 (0.04)
3 - Permanent crops	0.25	0.20 (0.04)
4 - Coniferous forest	2	2.91 (0.56)
5 - Deciduous forest	2	2.55 (0.51)
6 - Water	0.002	-
7 - Urban	2	0.92 (0.20)
8 - Other	0.05	0.19 (0.05)
9 - Desert	0.013	-

Table 5: Roughness length values from different types of studies. The first column states the global land use category of the z_0 values. The second column states the (range of) z_0 values, as well as the specific type of land use they are derived for. The third column shows the reference ([1]Literature study, [2]Model input (EMEP MSC-W), [3]Model input (CHIMERE)).

Land use categories	Proposed z_0 values (type name)	Reference
Grass	0.008 – 0.03 (short grass, moss)	Wieringa (1993) [1]
	0.02 – 0.06 (long grass, heather)	
	0.03 – 0.6 (categories DEPAC 1)	Silva et al. (2007)
	0.022 (short grassland)	Gallagher et al. (2002)
	0.063 (long grassland)	
	0.01 (mown grass)	Troen and Petersen (1989)
	0.03	Simpson et al. (2012) [2]
	0.1 (grassland)	Mailler et al. (2017) [3]
	0.013 (mean DEPAC 1)	This study
Arable land / permanent crops	0.04 – 0.09 (low mature crops)	Wieringa (1993) [1]
	0.12 – 0.18 (high mature crops)	
	0.05 – 0.5 (categories DEPAC 2)	Silva et al. (2007)
	0.1 – 0.5 (categories DEPAC 3)	
	0.12 (arable crop)	Gallagher et al. (2002)
	0.03 - 0.1 (farmland)	Troen and Petersen (1989)
	0.1 – 0.2 (different types of crops)	Simpson et al. (2012) [2]
	0.05 – 0.15 (agriculture)	Mailler et al. (2017) [3]
	0.19 (mean DEPAC 2)	This study
	0.20 (mean DEPAC 3)	
Forests	0.8 – 1.6 (mature pine forests)	Wieringa (1993) [1]
	0.6 – 1.2 (categories DEPAC 4 & 5)	Silva et al. (2007)
	1	Troen and Petersen (1989)
	0.8 – 1	Simpson et al. (2012) [2]
	1	Mailler et al. (2017) [3]
	2.5	Gallagher et al. (2002)
	1.71 – 1.9 (oak and pine trees)	Lankreijer et al. (1993)
	1.70 – 2.29 (spruce and pine trees)	Yang and Friedl (2003)
	2.91 (mean DEPAC 4)	
	2.55 (mean DEPAC 5)	This study
Urban	0.4 – 0.7 (dense low buildings)	Wieringa (1993) [1]
	0.7 – 1.5 (regularly-built town)	
	0.005 – 1.3 (categories DEPAC 7)	Silva et al. (2007)
	0.5 – 1 (suburbs, city)	Troen and Petersen (1989)
	1	Simpson et al. (2012) [2]
	1	Mailler et al. (2017) [3]
	0.92 (mean DEPAC 7)	This study
Other	0.35 - 0.45 (continuous bushland)	Wieringa (1993) [1]
	0.03 – 0.1 (categories DEPAC 8)	Silva et al. (2007) [1]
	0.01 (heathland)	Gallagher et al. (2002)
	0.05 – 0.2 (moorland, scrubs, wetlands)	Simpson et al. (2012) [2]
	0.15 (scrubs)	Mailler et al. (2017) [3]
	0.19 (mean DEPAC 8)	This study

Table 6: Comparison of the computed z_0 values from FLUXNET observations and the corresponding satellite derived z_0 values. The table shows the mean and standard deviation of all z_0 values in one year. For forest, only the maximum z_0 value is given.

Site ID	Land use	Computed z_0	Satellite-derived z_0
DE-Hai	DBF	2.3 (0.88)	3.5
FR-Fon	DBF	2.9 (0.53)	2.6
DE-Obe	ENF	1.9 (0.52)	3.4
DE-Tha	ENF	2.6 (0.72)	3.1
NL-Loo	ENF	2.8 (0.43)	2.3
BE-Bra	MF	2.8 (0.69)	2.4
BE-Vie	MF	4.7 (1.5)	3.0
CH-Lae	MF	3.5 (0.92)	3.8
DE-Akm	WET	0.72 (0.21)	0.14 (0.033)
DE-SfN	WET	0.46 (0.13)	0.22 (0.033)
CZ-wet	WET	0.16 (0.075)	0.18 (0.040)
BE-Lon	CRO	0.013 (0.018)	0.16 (0.029)
DE-Geb	CRO	0.020 (0.020)	0.17 (0.025)
DE-Kli	CRO	0.043 (0.043)	0.18 (0.030)
DE-RuS	CRO	0.066 (0.048)	0.15 (0.015)
DE-Seh	CRO	0.034 (0.028)	0.16 (0.015)
CH-Oe2	CRO	0.084 (0.065)	0.19 (0.019)
DE-RuR	GRA	0.035 (0.019)	0.014 (0.0016)
NL-Hor	GRA	0.14 (0.076)	0.014 (0.0019)
CH-Cha	GRA	0.078 (0.038)	0.015 (0.00099)
CH-Fru	GRA	0.13 (0.086)	0.015 (0.0024)
CH-Oe1	GRA	0.0064 (0.0035)	0.014 (0.00088)

865

Table 7: Relative change (%) in total N_r deposition w.r.t. the default run over Germany, the Netherlands and Belgium in 2014 per land use class.

	LE_{LAI}	LE_{z0}	LE_{z0+LAI}
Grass (1)	-5.34	-3.95	-8.05
Arable land (2)	9.53	3.27	12.88
Permanent crops (3)	0.22	-3.17	-2.78
Coniferous forest (4)	-9.36	-0.86	-7.36
Deciduous forest (5)	1.15	1.93	1.83
Urban (7)	16.62	-0.37	6.53
Other (6,8,9)	3.45	0.58	3.31

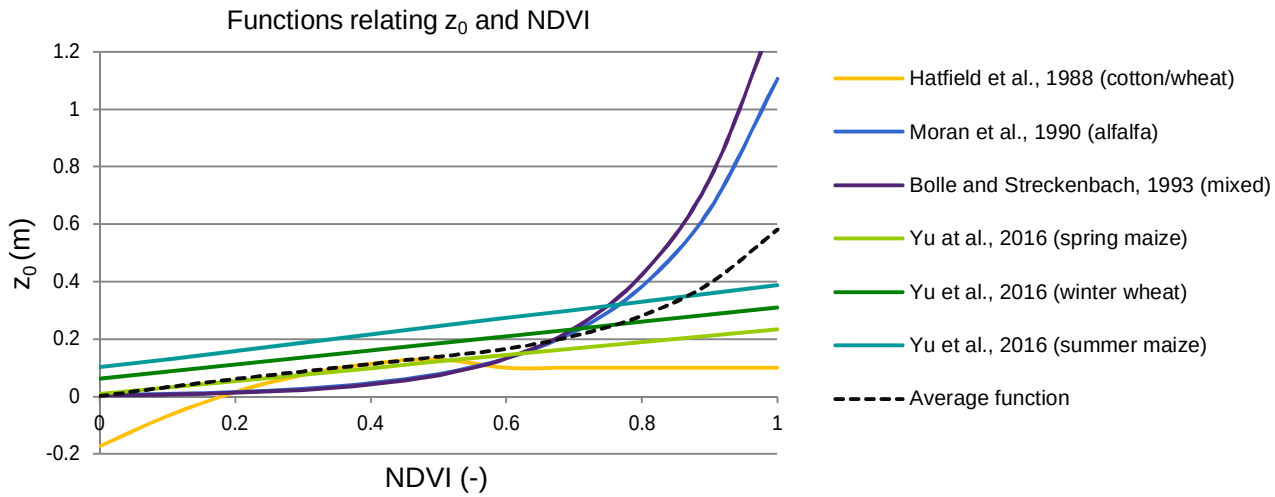

Figure 1: Several functions that relate the roughness length, z_0 (m) to the normalized difference vegetation index (NDVI). The dotted line shows the average of all the functions. This function is used to compute NDVI-dependent z_0 values for the subcategories within DEPAC classes “arable”, “other” and “permanent crops”.

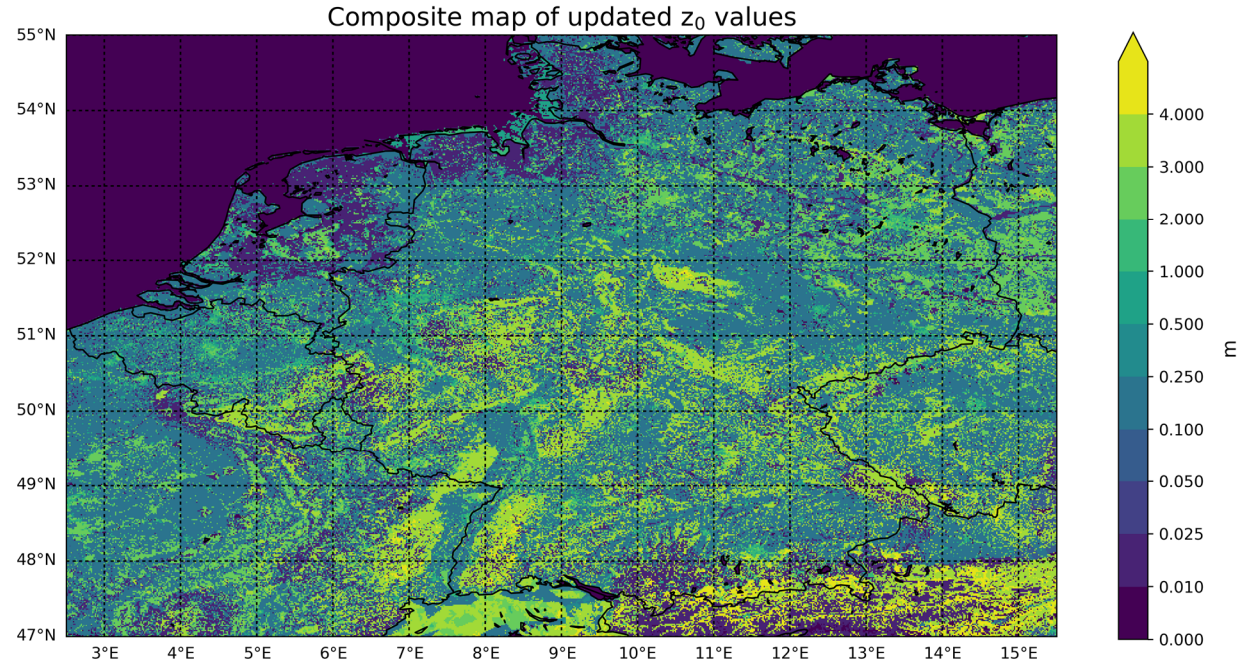

Figure 2: Composite map of the new z_0 values. The yearly mean is displayed for land use classes with time-variant z_0 values.

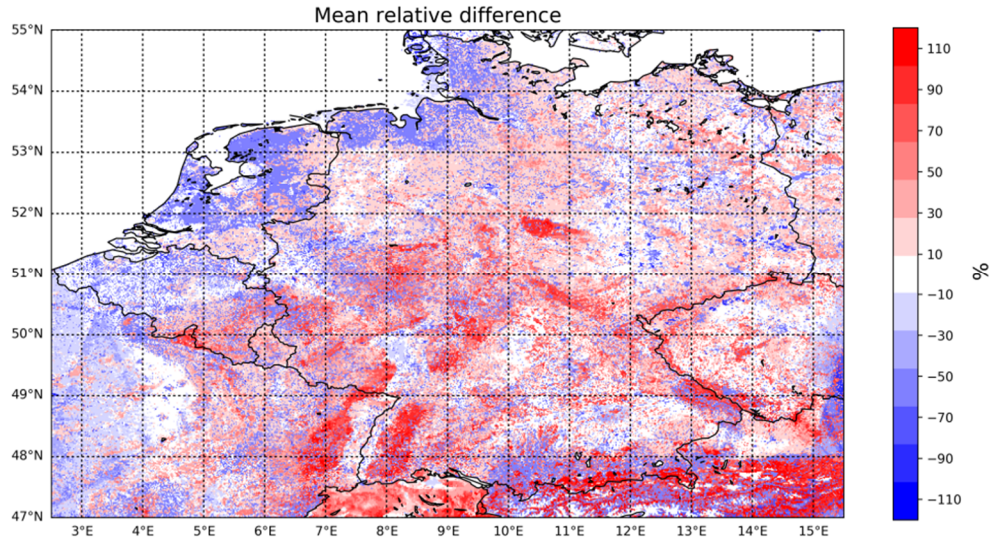

Figure 3: Mean relative difference (%) of the updated z_0 values with respect to the default z_0 values.

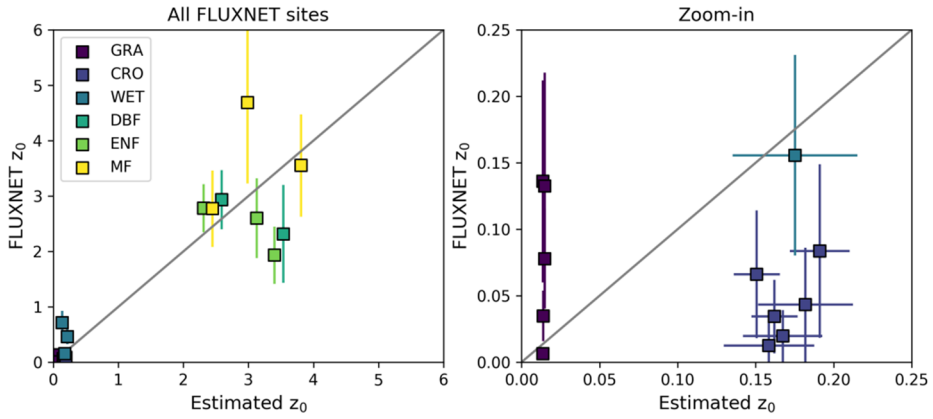

Figure 4: Comparison of the updated z_0 values (x-axis) to the z_0 values derived from EC measurements (y-axis). The error bars indicate the standard deviation.

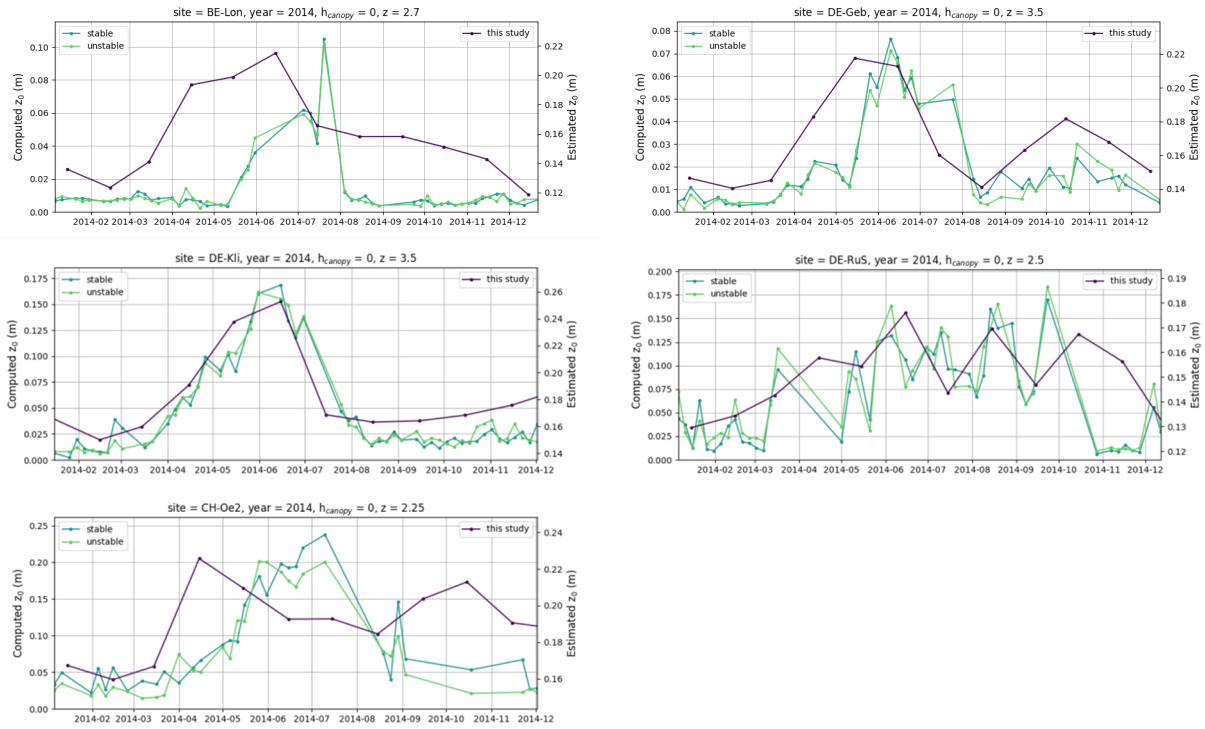

885 Figure 5: Seasonal variation of the computed z_0 values at the FLUXNET cropland sites in 2014 (left-axis), and the corresponding z_0 values estimated from NDVI-values (right-axis). The assumptions used to compute the z_0 values are shown in the titles of the figures.

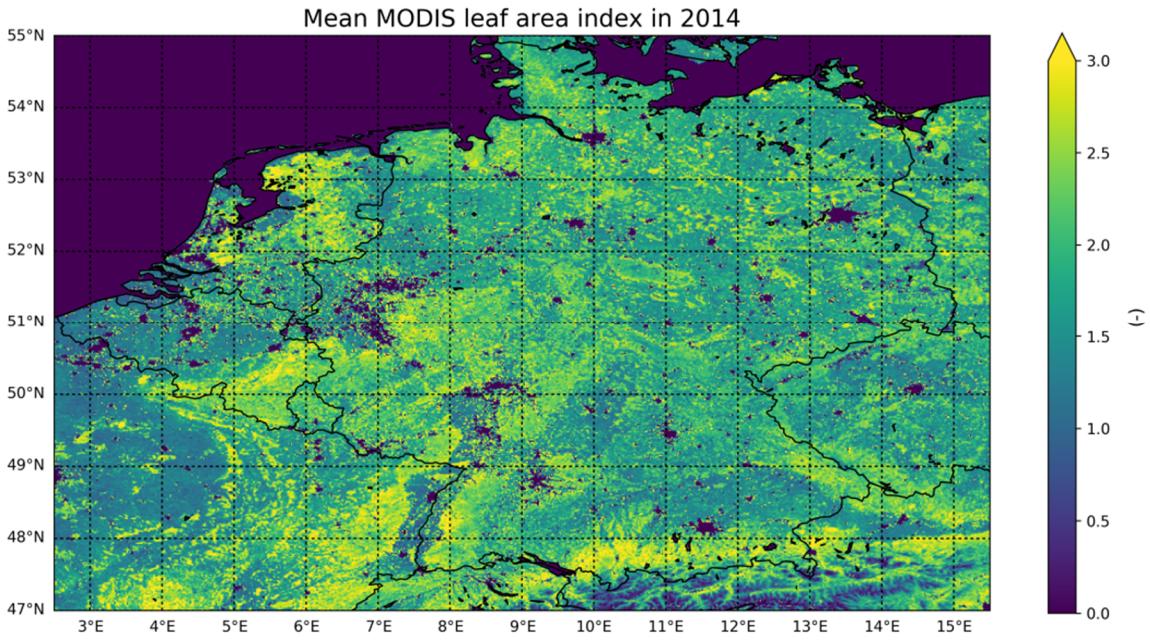

Figure 6: The yearly mean MODIS leaf area index in 2014.

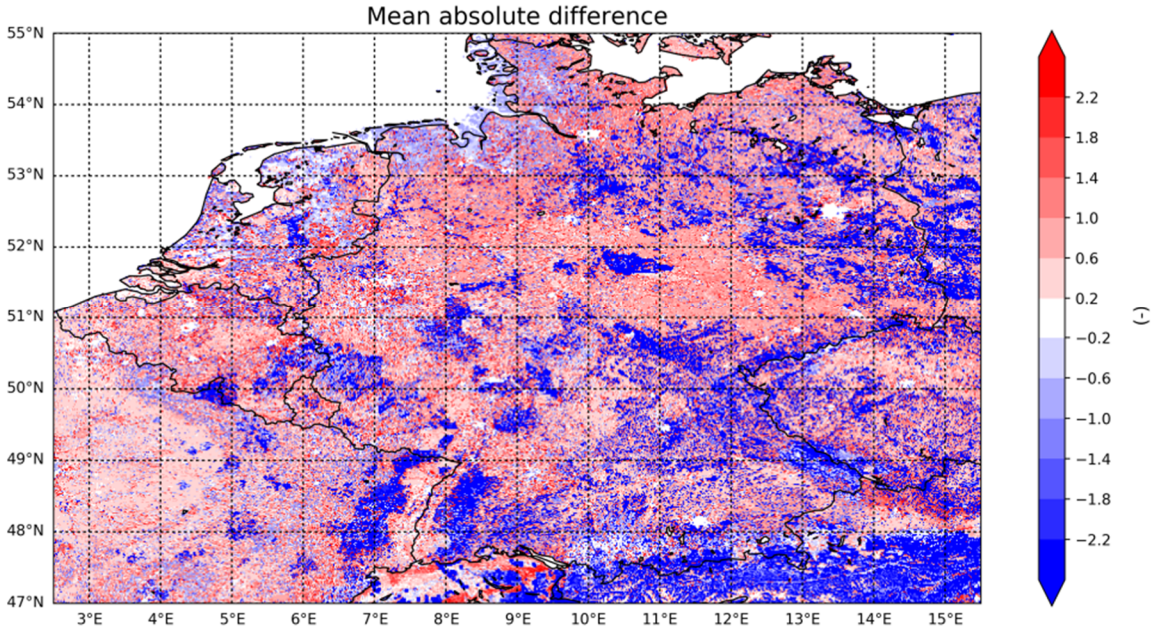

Figure 7: The absolute differences ($LAI_{MODIS} - LAI_{default}$) between the MODIS leaf area index and the default leaf area index in LOTOS-EUROS.

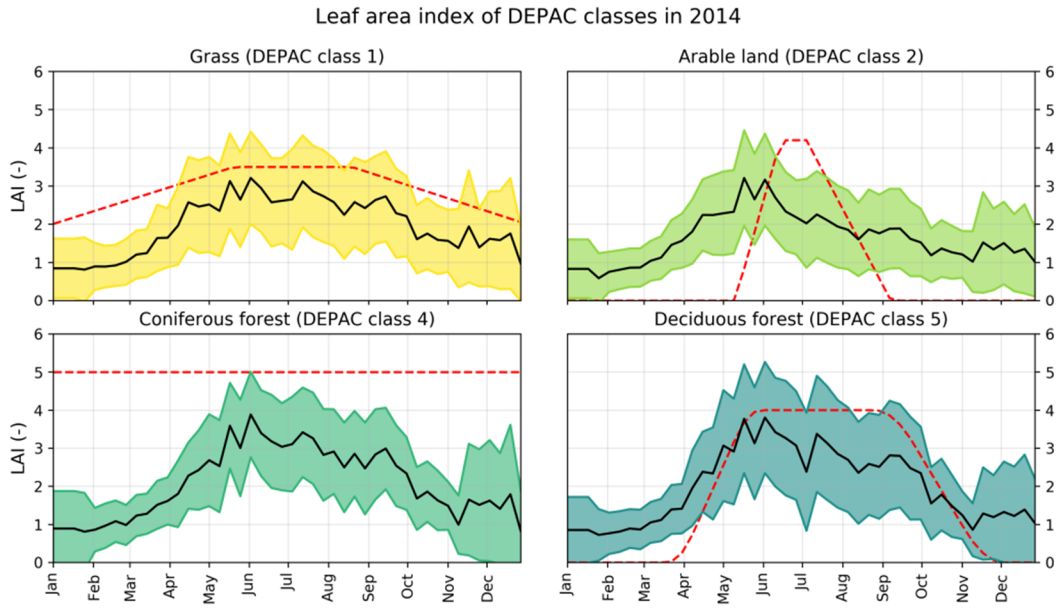

Figure 8: Seasonal variation of the default and MODIS-LAI values per DEPAC class. The black line represents the mean MODIS-LAI of all pixels within the modelled grid for that particular DEPAC class, the ranges represent the mean plus and minus the standard deviation of the MODIS-LAI. The red line depicts the default LAI values in LOTOS-EUROS.

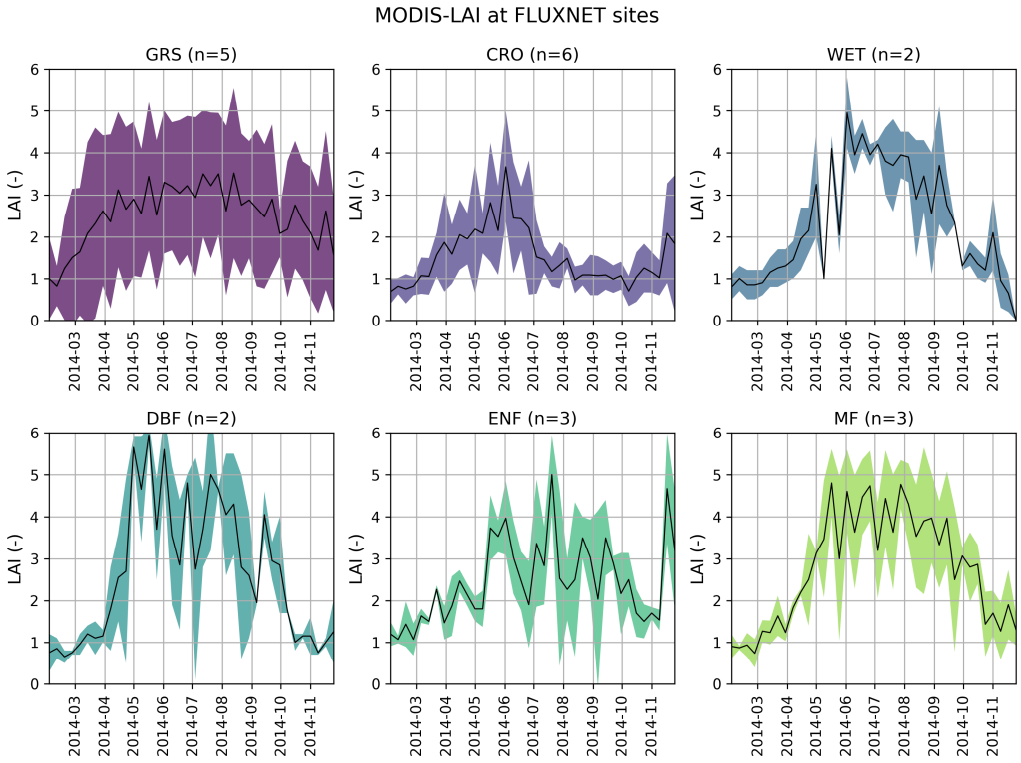

Figure 9: Seasonal variation of the MODIS-LAI at FLUXNET sites with different land use classifications. The black line represents the mean MODIS-LAI value per land use and the ranges represent the mean plus and minus the standard deviation.

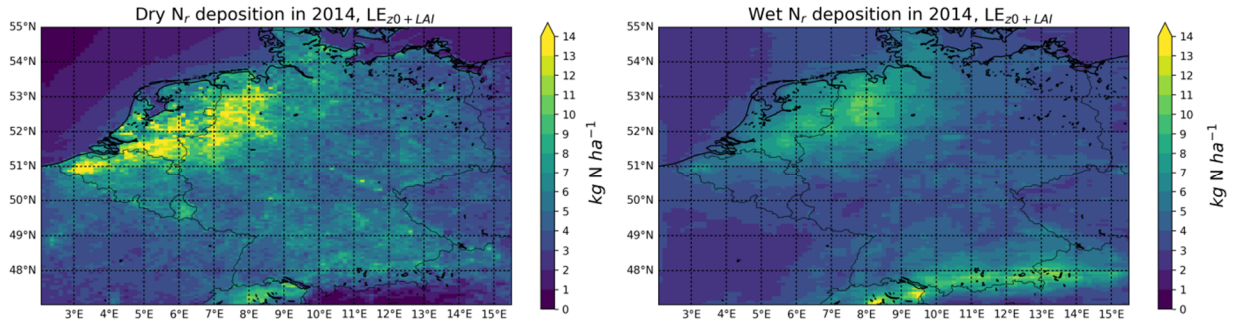

Figure 10: The modelled amount of dry (left) and wet (right) deposition in kg N ha^{-1} in 2014.

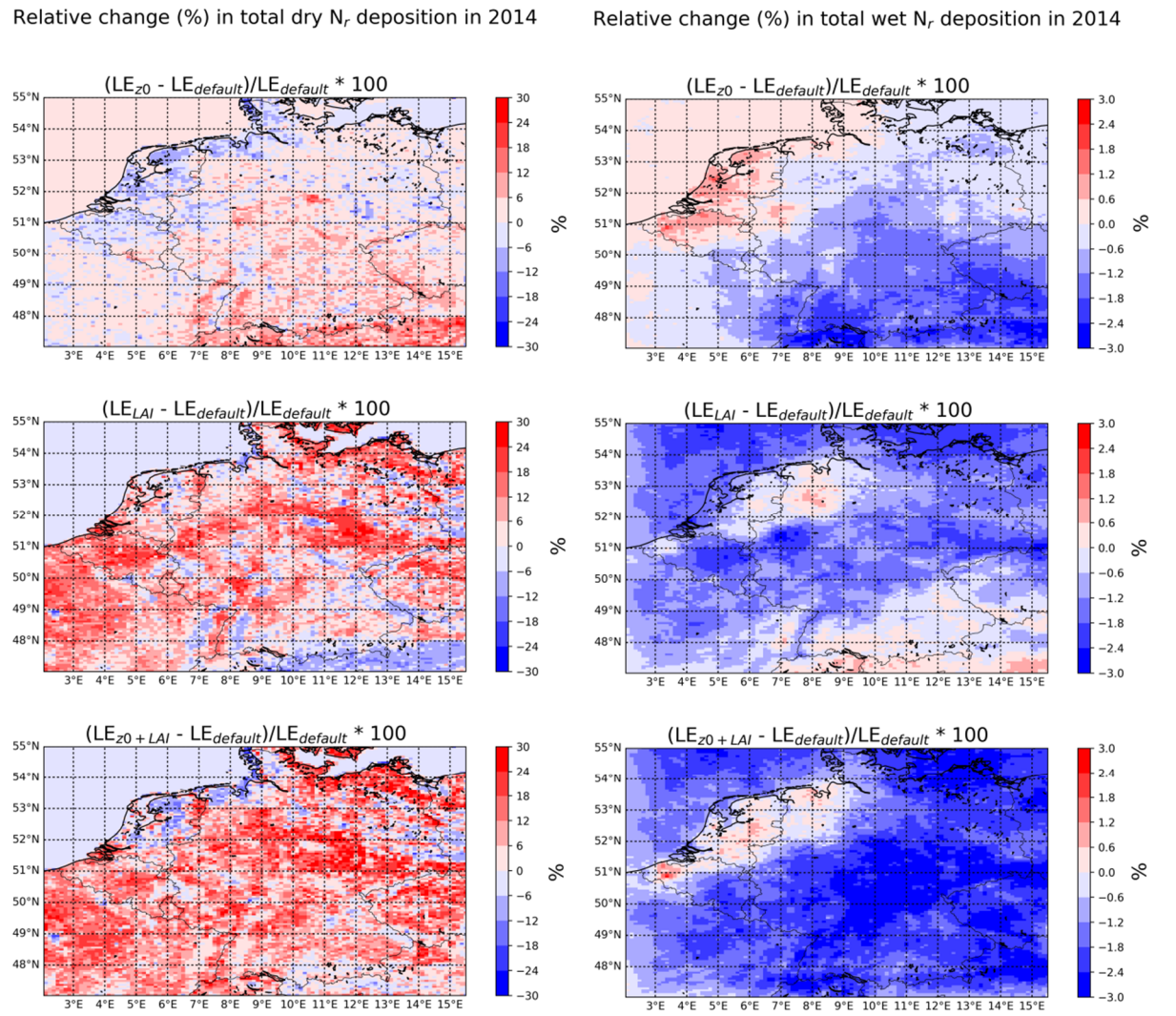

Figure 11: The relative change in total dry (left) and wet (right) N_r deposition in 2014 for the different model runs relative to the default LOTOS-EUROS run. The first row indicates the changes related to the implementation of the updated z_0 values. The second row indicates the changes related to the implementation of the MODIS LAI values. The third row shows the combined effect of both these updates. (Please note the different scales).

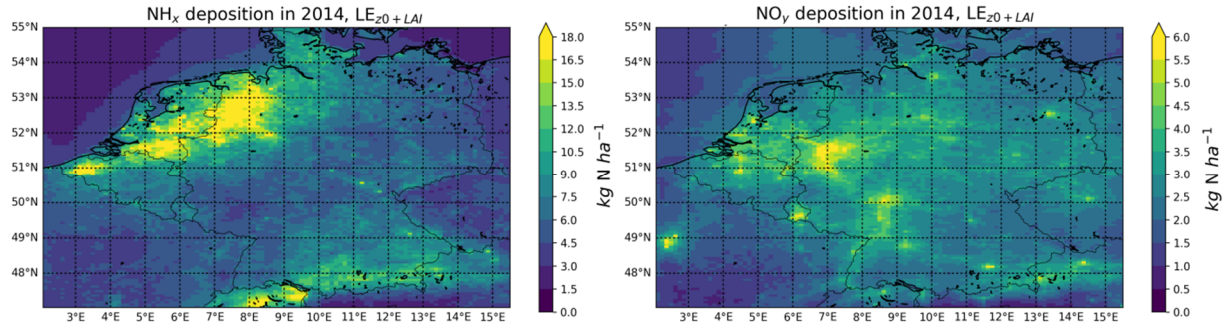

Figure 12: NH_x deposition (left) and NO_y deposition (right) in kg N ha^{-1} in 2014.

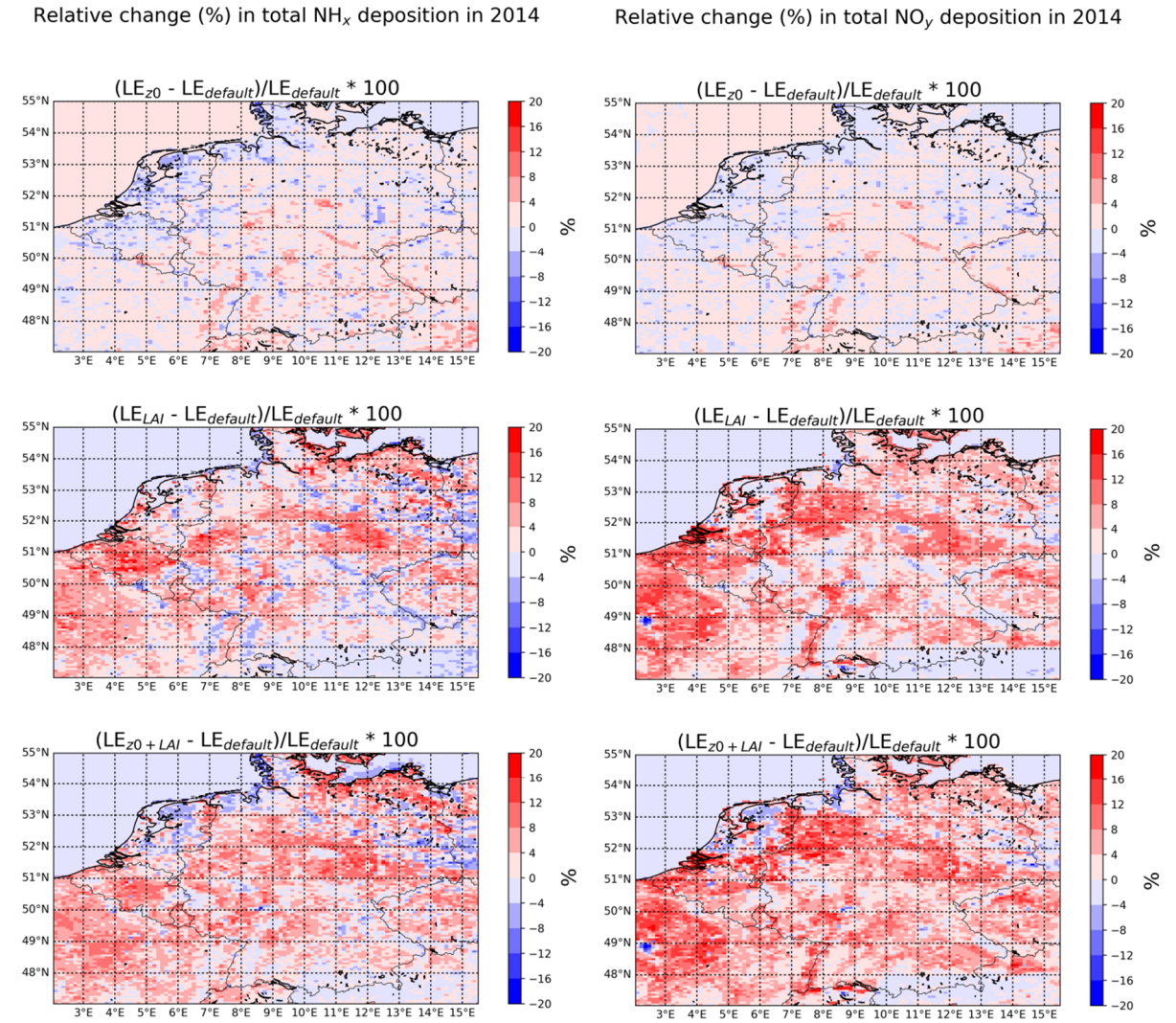

Figure 13: The relative change in total NH_x (top) and NO_y (bottom) deposition in 2014 for the different model runs relative to the default LOTOS-EUROS run. The first row indicates the changes related to the implementation of the updated z_0 values. The second row indicates the changes related to the implementation of the MODIS LAI values. The third row shows the combined effect of both these updates.

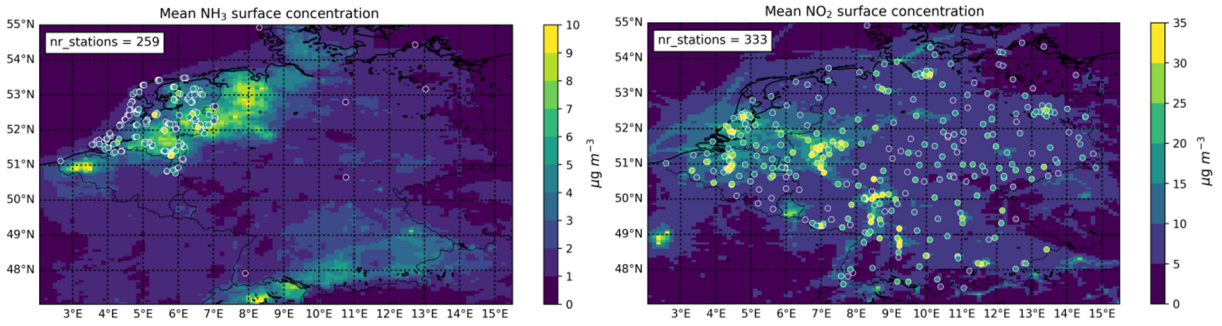

Figure 14: The yearly mean NH_3 (left) and NO_2 (right) surface concentrations in µg m^{-3} in 2014, and the corresponding mean surface concentrations measured at the in-situ stations.

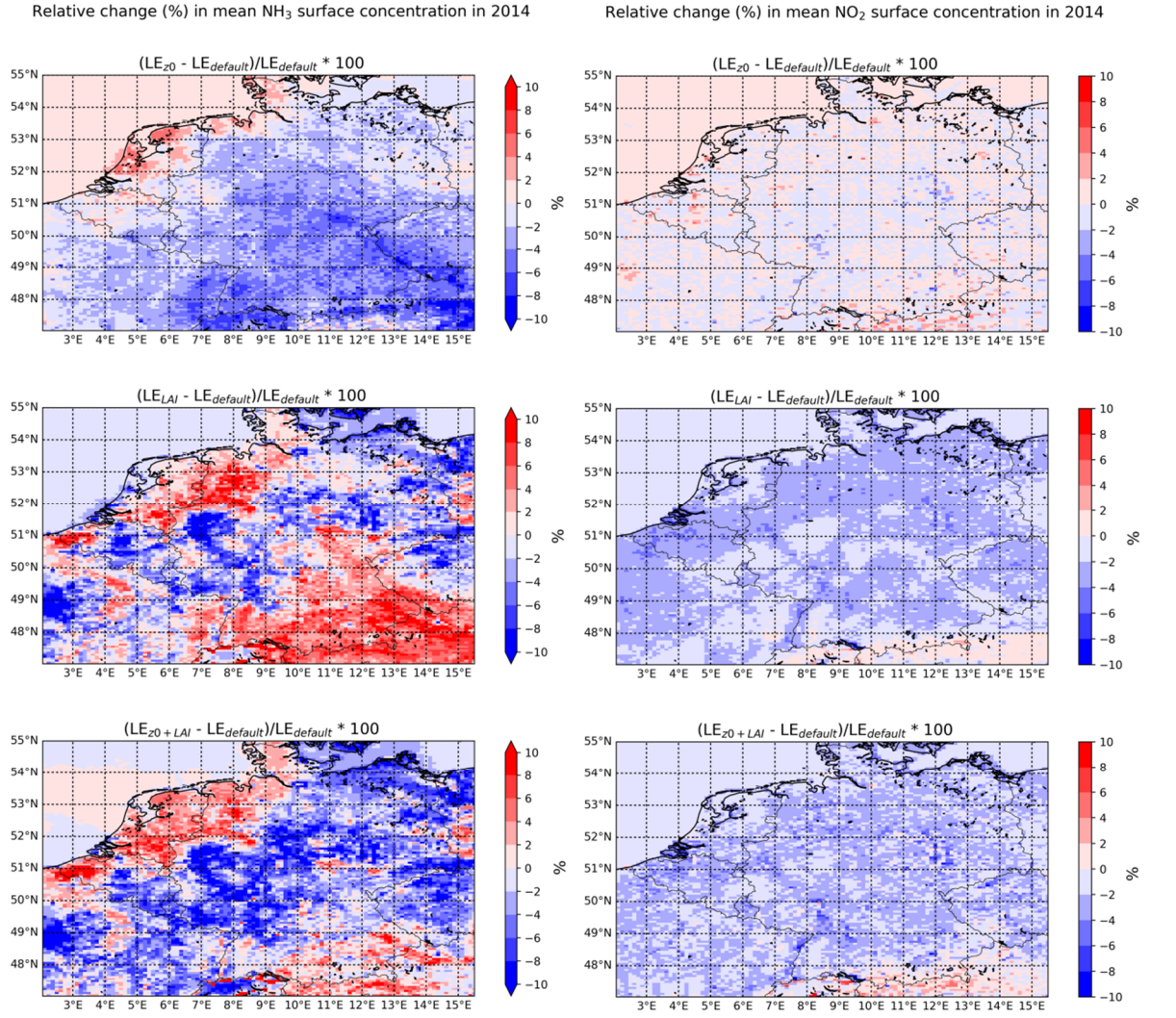

Figure 15: The relative change (%) in mean NH_3 (left) and NO_2 (right) surface concentration in 2014 for the different model runs relative to the default LOTOS-EUROS run. The first row indicates the changes related to the implementation of the updated z_0 values. The second row indicates the changes related to the implementation of the MODIS LAI values. The third row shows the combined effect of both these updates.

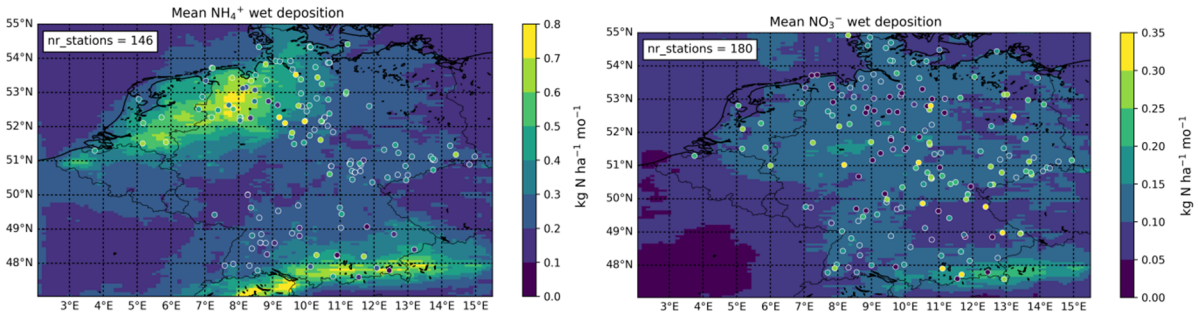

Figure 16: The mean NH_4^+ (left) and NO_3^- (right) wet deposition in kg N ha^{-1} mo^{-1} in 2014.The mean observed wet deposition observed at the stations is plotted on top.

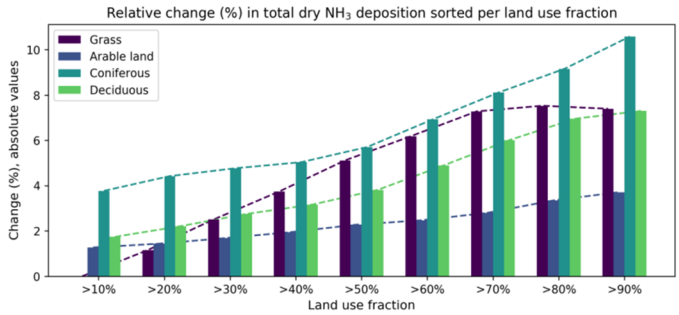

Figure 17: The relative difference (%) in total dry NH_3 deposition in 2014 between the default run ($LE_{default}$) and the run with the updated z_0 values (LE_{z0}), sorted by increasing land use fraction.

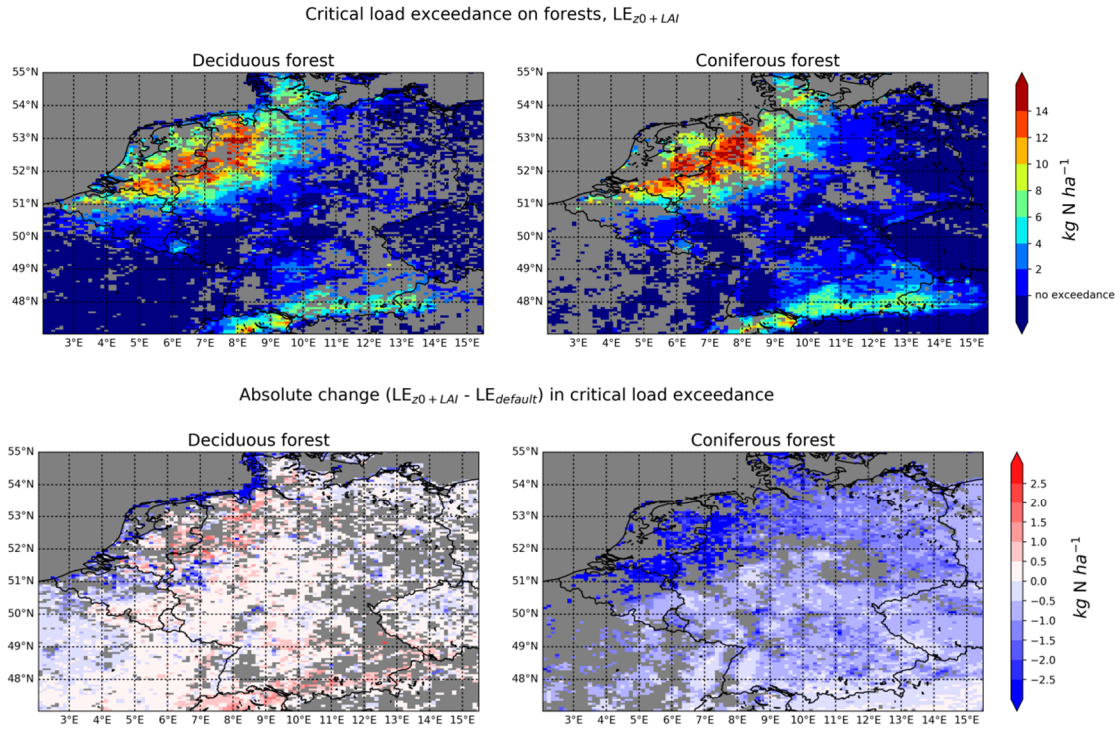

Figure 18: Critical load exceedances on forests in kg N ha^{-1} in 2014. The upper figures show the critical on deciduous (left) and coniferous (right) forest, as modelled with the updated z_0 and LAI values. The lower figures show the absolute differences in critical load exceedance on deciduous (left) and coniferous (right) between the new and the default LOTOS-EUROS run.